JGR Oceans

RESEARCH ARTICLE
10.1029/2018JC014687

Special Section:
The U.S IOOS Coastal and Ocean Modeling Testbed 2013-2017

U.S. IOOS Coastal and Ocean Modeling Testbed: Hurricane-Induced Winds, Waves, and Surge for Deep Ocean, Reef-Fringed Islands in the Caribbean

B. R. Joyce[1], J. Gonzalez-Lopez[2], A. J. Van der Westhuysen[3], D. Yang[3], W. J. Pringle[1], J. J. Westerink[1], and A. T. Cox[4]

[1]Department of Civil and Environmental Engineering and Earth Sciences, University of Notre Dame, Notre Dame, IN, USA, [2]Wood, E&IS, Met-Ocean Services, Dartmouth, Nova Scotia, Canada, [3]IMSG at NOAA/NWS/NCEP/Environmental Modeling Center, College Park, MD, USA, [4]Oceanweather Inc., Stamford, CT, USA

Key Points:
- Regional simulations show that Hurricanes Irma and Maria storm surge was largely driven by atmospheric pressure with local wind and wave effects
- High-resolution detail of physical structures such as reefs, shoals, and banks are important to simulating wave setup in deep ocean islands
- Sufficiently resolved regional-scale models adequately represent atmospheric pressure and wind-driven surge over narrow shelves

Supporting Information:
- Supporting Information S1
- Figure S1
- Figure S2
- Figure S3
- Figure S4
- Figure S5
- Figure S6
- Figure S7
- Figure S8

Corresponding to:
B. R. Joyce,
bjoyce@nd.edu

Citation:
Joyce, B. R., Gonzalez-Lopez, J., Van der Westhuysen, A. J., Yang, D., Pringle, W. J., Westerink, J. J., & Cox, A. T. (2019). U.S. IOOS coastal and ocean modeling testbed: Hurricane-induced winds, waves, and surge for deep ocean, reef-fringed islands in the Caribbean. *Journal of Geophysical Research: Oceans*, *124*, 2876–2907. https://doi.org/10.1029/2018JC014687

Received 26 OCT 2018
Accepted 24 MAR 2019
Accepted article online 1 APR 2019
Published online 29 APR 2019

Abstract As part of a U.S. Integrated Ocean Observing System (IOOS) funded Coastal and Ocean Modeling Testbed (COMT), hindcasts of waves and storm surge for 2017 Hurricanes Irma and Maria are examined and compared to wave and water level gauge data in the vicinity of Puerto Rico and the U.S. Virgin Islands. The region is characterized by adjacent deep ocean water, narrow shelves, and coral reef systems providing coastal protection. The storm physics are analyzed using an unstructured grid third-generation wave circulation coupled modeling system (ADCIRC+SWAN) with respect to tides, winds, atmospheric pressure, waves, and wave radiation stress-induced setup. The water level response is generally dominated by the pressure deficit of the hurricanes. Wind-driven surge is important over the shallow shelf to the east of Puerto Rico and wave-induced setup becomes significant at locations in close proximity to the coastline. Contrary to conditions along the Gulf of Mexico shelf, geostrophically induced setup is negligible. Characteristics from a range of meteorological forcing models are assessed, and the associated errors in the hydrodynamic response are quantified. A data-assimilated tropical planetary boundary model leads to the smallest atmospheric pressure, water level and wave property errors across both storms. Through comparisons between ADCIRC+SWAN and SLOSH-FW (a structured grid first-generation wave circulation coupled model), it is shown that the response to atmospheric forcing is similar; however, nearshore wave setup is smaller in SLOSH-FW due to its coarser resolution here. Further, in addition to erroneous wind-driven surge through depth limiting over the open ocean, numerical oscillations in the water level time series develop in SLOSH-FW likely due to its small domain size.

1. Introduction

This study focuses on the prediction of tides and hurricane-driven storm surge and waves adjacent to deep ocean islands, specifically examining Puerto Rico (PR) and the U.S. Virgin Islands (USVI), a region dramatically impacted by Hurricanes Irma and Maria in 2017. These often reef-fringed islands appear in coastal environments that differ substantially in their surrounding bathymetric profiles and the scale of their inland bays and estuaries from environments found along continental shelves. PR and USVI sit on an underwater mountain range which separates the Caribbean Sea and the Atlantic Ocean with a narrow shelf with depths of 20–50 m, which abruptly drop to 3,000 m and deeper. This region experiences an especially high occurrence of intense tropical storms and hurricanes as these storms form between 5 and 30° north latitude in the Atlantic and move toward the west, in the direction of PR and USVI (https://www.nhc.noaa.gov/climo/). The resulting hazardous coastal conditions can differ substantially from those which occur in coasts situated on broad continental shelves. Due to the lack of a broad shelf to dissipate wave energy, waves are often much larger at the coasts of these deep ocean islands, leading to larger wave radiation stresses and increased wave run-up (Kennedy et al., 2012). Additionally, the larger bathymetric depths can limit the wind-driven component of storm surge, and the steep gradients between the deep ocean and the narrow island shelves and the intricate reef structures make the coastal hydrodynamics of this region particularly interesting.

In previous studies, significant attention has been paid to mild-sloped and broader continental shelf regions with complex inland coastal environments. More specifically, the U.S. Integrated Ocean Observing System

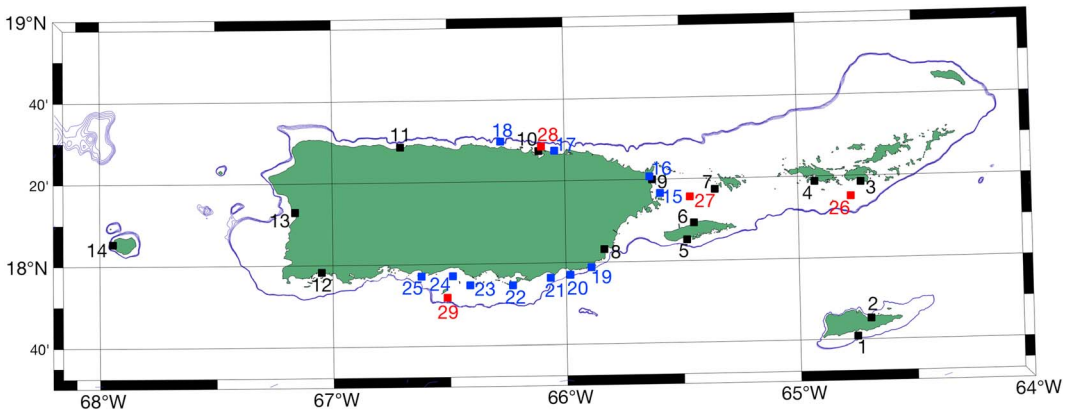

Figure 1. The Puerto Rico and U.S. Virgin Islands study region. The 100- to 200-m bathymetric contour is highlighted showing the location of the island shelves. Numbers correspond to locations listed in Table 1.

(IOOS) funded Coastal and Ocean Modeling Testbed (COMT; Luettich et al., 2013) studies (Hope et al., 2013; Kerr, Donahue, et al.,2013; Kerr, Martyr, et al.,2013; Zheng et al., 2013) analyzed storm surge and wave processes on broad shelved areas in the Gulf of Mexico through hindcasts of Hurricanes Rita (2005) and Ike (2008). Three unstructured grid storm surge (ADCIRC, FVCOM, and SELFE) and wind wave (SWAN, WWMII) models, in addition to National Oceanic and Atmospheric Administration's (NOAA) structured grid forecast storm surge model (SLOSH) were intercompared. The studies showed that storm surge on mild-sloped shelves is dominated by wind effects. Due to attenuation over the broad shelf, wave setup effects have a small but nonnegligible contribution. Additionally, the importance of geostrophically induced forerunner was noted, particularly for Hurricane Ike (Hope et al., 2013; Kennedy et al., 2011). Each of the unstructured grid models are similarly skillful at reproducing the observed storm surge and wave environment for these storms, while SLOSH generally underestimates surge with 2–3 times greater high water mark errors than the unstructured grid models and cannot account for the Ike forerunner (Kerr, Donahue, et al.,2013). Further, it was found that model resolution is relatively unimportant for capturing tidal signals in the open ocean, but very important to the representation of hurricane surge and wave responses, within intertidal zones, the nearshore, and inland coastal areas (Kerr, Martyr, et al.,2013). Bottom friction representations were likewise important to the primary and forerunner surge representation on the continental shelf (Hope et al., 2013; Kerr, Martyr, et al.2013; Zheng et al., 2013). Additional model studies have used a number of different models to look at the regionally specific physics influencing coastal water levels in broad shelved regions. These include detailed investigations into geostrophic currents which develop on the continental shelf (Bilskie et al., 2016; Kennedy et al., 2011) and uncertainties in surge modeling due to land cover specification in the Gulf of Mexico (Ferreira et al., 2014), as well as analysis of wave-current interactions and nearshore hydrodynamics during extratropical events in New England (Chen et al., 2013; Xie et al., 2016).

Recently, the COMT program has been expanded to consider deep ocean islands and examine NOAA's existing operational models used to predict hazardous surge and wave conditions that occur there (Luettich et al., 2017; van der Westhuysen et al., 2015). Currently, there is a research and knowledge gap with respect to storm surge response for these islands. This knowledge gap is compounded by a historical lack of rich observational data for landfalling hurricane events on these islands, which has recently been rectified and is leveraged here. Since 2011, the IOOS Caribbean Coastal Ocean Observing System (CARICOOS, https://www.caricoos.org/) has deployed a number of buoys, coastal meteorological stations, and HF-Radar networks in the PR and USVI region (Canals et al., 2012; Morell et al., 2015). The U.S. Geological Survey (USGS) has invested in rapid deployment on-shore water level and atmospheric pressure gauges that were in place for Hurricane Maria (https://stn.wim.usgs.gov/fev/#MariaSeptember2017). These new assets supplement the existing permanent NOAA-deployed regional water level gauges, anemometers, and atmospheric pressure gauges (https://tidesandcurrents.noaa.gov/). Figure 1 shows the location of the NOAA water level and meteorological stations, the CARICOOS wave buoys, and the USGS rapid deployment gauges used for validation, listed in Table 1. These elements enable the design, evaluation, and advancement of operational tide, wave, currents, and storm surge models in U.S. island regions (Canals & Morell, 2015; Gonzalez-Lopez

Table 1
All Water Level, Meteorological (NOAA/NOS and USGS), and Wave Data (CARICOOS) Validation Stations

Water level	Region	Number
NOAA/NOS		
Lime Tree Bay	C	1
Christiansted	C	2
Lameshur Bay	VI	3
Charlotte Amalie	VI	4
Esperanza	E	5
Isabel Segunda	E	6
Culebra	E	7
Yabucoa	E	8
Fajardo	E	9
San Juan	N	10
Arecibo	N	11
Magueyes	S	12
Mayaguez	W	13
Mona	W	14
USGS		
Ceiba	E	15
Fajardo	E	16
SJ	N	17
Dorado	N	18
Maunabo	S	19
Patillas	S	20
Arroyo	S	21
Salinas	S	22
Santa Isabel	S	23
Juana Diaz	S	24
Ponce	S	25
CARICOOS		
VI 1	VI	26
PR 3	E	27
PR 2	N	28
PR 1	S	29

Note. Regions are denoted as follows: C for Caribbean, VI for the Virgin Islands, E for eastern Puerto Rico, N for northern Puerto Rico, S for southern Puerto Rico, and W for western Puerto Rico. Numbers correspond to locations shown on Figure 1.

et al., 2017; Pomales-Velázquez et al., 2015; Rodríguez-Abudo et al., 2015), via a close collaboration between federal operational, model development, and data management partners.

In September 2017, Hurricanes Irma and Maria had an unprecedented impact on the Caribbean region through wind, storm surge, and wave damage. Due to the existing observational capabilities in the region, ocean and meteorological observations were captured as both Hurricanes Irma and Maria passed through the region (Chardon-Maldonado et al., 2018). This allowed for a close study of the impact of these high-intensity hurricanes on the coasts of PR and the USVI. One of the strongest storms in recent history, Hurricane Irma passed through the Caribbean Islands on 6 September 2017 as a Category 5 hurricane and had a catastrophic impact on the island of Barbuda and the British Virgin Islands where landfall was made. After landfall in the Virgin Islands, Irma passed approximately 50 miles to the north of San Juan, PR, and generated up to 1 m of storm surge and large waves on the northern coast of PR (Cangialosi et al., 2018). While slightly weaker in intensity than Irma, Hurricane Maria's track directly over PR led to conditions for the island which caused damage unprecedented in recent times. Maria made direct landfall over the southeast coast of PR near the town of Yabucoa causing well over a meter of storm surge along sections of the eastern coast of PR (Pasch et al., 2018).

This study seeks to continue the investigations performed in previous COMT studies, with a focus toward reef-fringed deep ocean island environments. The main aim is to understand the physics of storm surge and waves in the region under hurricane conditions using the coupled ADCIRC+SWAN model simulated on a high-resolution regional-scale mesh forced with assimilated meteorology (section 3.1). In particular, we design a set of experiments to determine the relative contributions model forcings (tides, inverted barometer response to atmospheric pressure, wind-induced surface stresses, and wind wave setup or setdown) on water levels. Additionally, various meteorological products are tested to determine their impact on water levels and model skill in section 3.2. Due to operational requirements, simplified models simulated on small-scale domains are often used. Thus, in section 3.3 and experimental version of SLOSH, which is coupled to a simplified wave model (FW), is compared with ADCIRC+SWAN to determine its applicability to the PR and USVI region and to evaluate the importance of model aspects such as deep ocean depths, resolution, and computational domain size. A discussion of the storm surge and wave response to the various hurricane forcing components is given in Section 4, with an emphasis on the effect and modeling implications of the narrow, steep shelf environment of the region.

2. Model, Data and Experimental Description

This study employs combinations of coastal flood, wind wave, and atmospheric models to assess coastal water levels due to hurricane forcing as detailed in Table 2. The preferred combination used for most of our analyses is ADCIRC+SWAN+OWI, which gave the best agreement with observations. In this configuration ADCIRC (coastal flood circulation model) is fully coupled to SWAN (third-generation wind wave model) in which they are computed on the same high-resolution unstructured triangular mesh (Dietrich et al., 2011). OWI is a data-assimilated wind product with a high-resolution structured grid nest covering Puerto Rico and the US Virgin Islands. Mean sea surface pressures and 10-m winds from OWI are read into ADCIRC+SWAN and applied as barometric pressure and surface stresses, respectively. The unstructured mesh employed by ADCIRC+SWAN model can be applied over the wide range of scales of motion and hydrodynamic processes that exist when computing the flow of water from the deep ocean to the nearshore, and then into coastal estuaries and onto coastal floodplains. The computations are implemented in a parallel processing framework that is highly scalable to tens of thousands of processing cores (Dietrich et al., 2012; Tanaka et al., 2011).

Journal of Geophysical Research: Oceans

10.1029/2018JC014687

Table 2
Description of the Storm Surge, Wind Wave and Atmospheric Forcing Models Used in This Study

Model acronym	Model name	Type and numerical scheme	Processes modeled	Mesh resolution	Domain extents	Time step	References
Storm Surge Models							
ADCIRC	ADvanced CIRCulation v53	shallow water equations, finite-element on unstructured triangles	tides, surge, wind wave setup	30 m to 15 km	Atlantic Ocean west of 60° W meridian	1 s	Luettich and Westerink (2004) and Westerink et al. (2008)
SLOSH	Sea, lake, and Overland Surges from Hurricanes	shallow water equations, finite-difference on structured curvilinear grid	surge, wind wave setup	90 m to 1 km	Puerto Rico and Virgin Islands	3 s	Jelesnianski (1967) Jelesnianski et al. (1992)
Wind Wave Models							
SWAN	Simulating WAves Nearshore	third-generation spectral action balance equations, unstructured triangles	40 frequencies (0.05 Hz to 3 Hz) in 36 directions	same as ADCIRC	same as ADCIRC	10 min	Booij et al. (1999) Zijlema (2010)
FW	Fast Wave	first-generation spectral action balance equations, structured grid	two carrier frequencies (wind waves and swell) in 8 directions	1 km	rectangular domain enclosing SLOSH domain	60 min	Schwab et al. (1984)
Atmospheric Forcing Models							
OWI	Oceanweather Inc.	assimilated tropical planetary boundary layer model	synoptic and tropical cyclone winds and pressure	0.02° (Maria), 0.05° (Irma), and 0.25° nests	North Atlantic Ocean, Puerto Rico focused inner nests	15 min	Cox et al. (2017)
HWRF	Hurricane Weather Research and Forecasting	assimilated coupled atmosphere-ocean model with vortex modification	synoptic and tropical cyclone winds and pressure	2 km, 6 km, and 18 km nests	North Atlantic Ocean, storm following inner nests	1 hr	Biswas et al. (2017) Yablonsky et al. (2015)
AHPV	Asymetric Holland Parametric Vortex	parametric based on ATCF best-track data	tropical cyclone winds and pressure	analytical	size of storm	6 hr	Mattocks and Forbes (2008)
CFSv2	Climate Forecast System version 2	assimilated coupled atmosphere-ocean-land reanalysis model	synoptic winds and pressure	0.2° (winds), 0.5° (pressure)	quasi-global	1 hr	Saha et al. (2014)

Note. The components of the preferred model configuration (ADCIRC+SWAN+OWI) are emboldened.

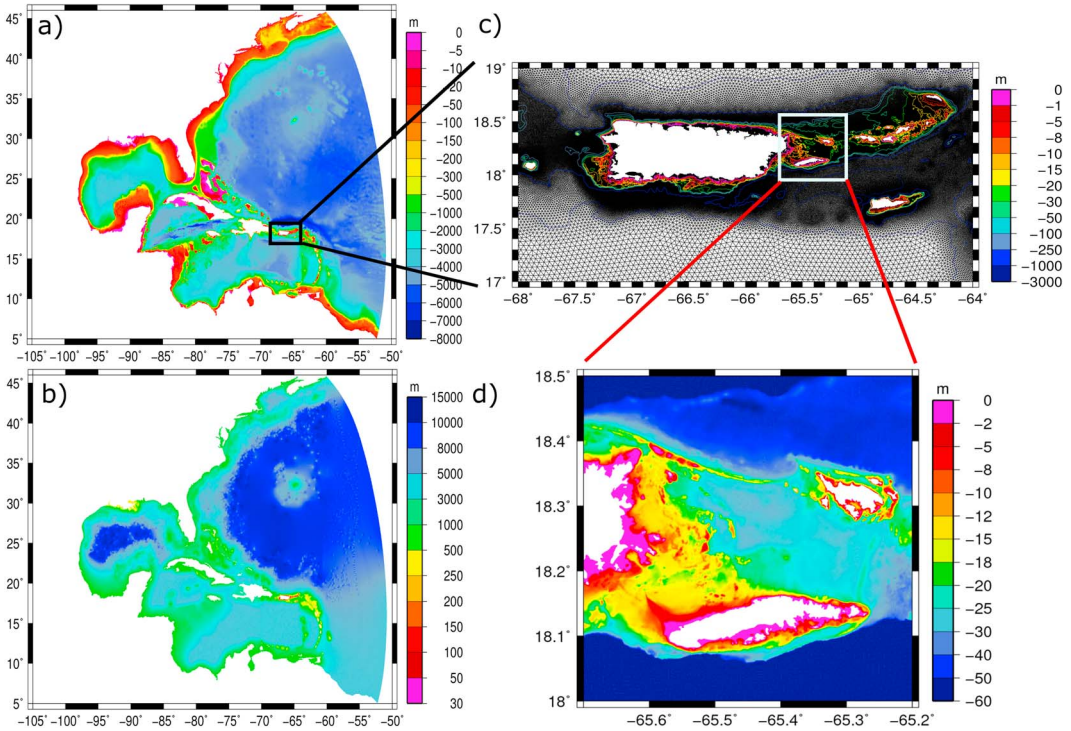

Figure 2. ADCIRC+SWAN PRVI15 computational mesh. The bathymetry and mesh element size in the entire model domain are shown in (a) and (b), respectively. Details of the mesh and model bathymetry in the study domain are shown in (c), and detail of eastern Puerto Rico, the island of Vieques, and the shallow shelf and reef system are shown in (d).

2.1. ADCIRC+SWAN Model Setup and Mesh Design

A high-resolution mesh (Figure 2), henceforth called PRVI15, was constructed based on the EC2001 grid (Mukai et al., 2002). The original spatial resolution of EC2001 was doubled throughout the entire mesh and additional details were added in the Caribbean Sea, with an emphasis on the Lesser Antilles, Puerto Rico, and the Virgin Islands in order to better represent the narrow and steep shelves, ridges, and banks here. Spatial resolution is coarsest (~15 km) in the deep ocean regions of the North Atlantic and Gulf of Mexico basins and finest (~30–100 m) along the PR and USVI coastlines (Figures 2 and 3). The highest level of resolution is applied to sharply define reef systems and complex coastline details and extends inland onto the floodplains. PRVI15 has a total of 2,723,449 vertices and 5,373,139 triangular elements.

The baseline bathymetry for the Caribbean Sea was obtained from the General Bathymetric Chart of the Oceans (GEBCO; specifically, the GEBCO_2014 Grid, version 20150318, www.gebco.net). Additional finer bathymetry for the Lesser Antilles was obtained from the SRTM30_PLUS data set (Becker et al., 2009) and nautical charts. Coastlines were defined using the GSHHG data set (Wessel & Smith, 1996). For PR and USVI a 10-m topobathy digital elevation model (Taylor et al., 2008) is used to obtain a detailed representation of nearshore and overland regions, in addition to submarine features such as reefs, sand banks, and steep shelf breaks (Figures 2c and d). Figure 2d highlights the reef system that extends from the northeast corner of PR to the island of Culebra.

Tidal forcing was provided at the mid-Atlantic open ocean boundary by applying the tidal surface elevation amplitudes and phases (constituents M_2, K_2, N_2, S_2, K_1, Q_1, P_1, and O_1) obtained from the TPXO8 global tidal solution (Egbert et al., 1994). In addition, an inverted barometer coinciding with the atmospheric pressure deficit was added to the tidal boundary forcing signal on the open ocean boundary. Within the domain, tidal potential functions drive the gravitational tidal body forces using the same constituents as are forced on the open ocean boundary. For SWAN, a spectral directional resolution of 10° was used. The frequency range for the SWAN model is from 0.05 to 3 Hz, logarithmically distributed over 40 bins. A Courant Friedrichs Lewy (CFL) limiter of 0.5 was used to limit propagation on the frequency and direction domains to avoid unphysical, numerical-induced refraction over the sharp gradients of the steep shelves (Dietrich et al., 2013).

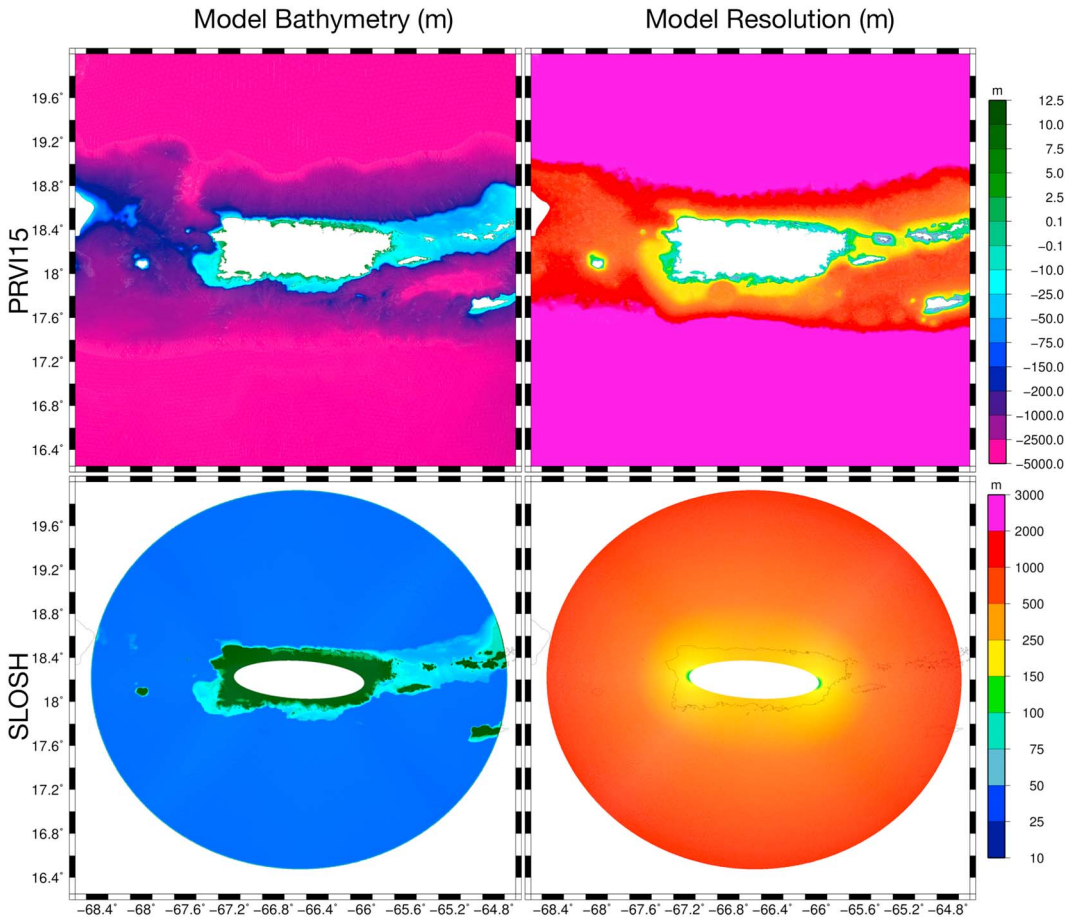

Figure 3. Comparison of model bathymetry (m) and model resolution (m) between the PRVI15 computational mesh and the SLOSH computational grid.

Wave breaking and bottom friction were parameterized using Ruessink et al. (2003) and Madsen et al. (1989), respectively.

Surface stresses are computed from 10-m winds using Garratt's drag law (Garratt, 1977) with an upper limit on the drag coefficient set to 0.0035 to account for sheeting at hurricane-level wind speeds. Often sector-based drag coefficients such as Powell et al. (2003) are used in the presence of hurricane force winds. Approaches such as this are difficult to apply to atmospheric forcings not defined by a storm track (such as CFSv2 and OWI wind fields used in this study), and therefore, this approach was not used. Wind input is uniformly applied throughout the ADCIRC+SWAN model domain. ADCIRC shares the 10-m wind speed forcing with SWAN in order to facilitate the calculation of wave generation in deep water and in the nearshore. Bottom friction is parameterized in ADCIRC using a quadratic bottom stress, where the bottom drag coefficient is dependent on the Manning's n coefficient and depth at each mesh node (Kerr, Martyr, et al.2013). Correct nearshore and overland frictional representation is critical to accurately simulating peak coastal water levels and inundation (Ferreira et al., 2014). A Manning's n of 0.025 and 0.028 was used for the Atlantic Ocean and the Caribbean Sea, respectively. Reefs and mangroves cover an extensive area near Caribbean islands, serving as natural barriers and providing dissipation and protection from the nearshore to the shelf edge. To account for their frictional effects, global maps of reef and mangrove coverages (Giri et al., 2011; Kendall et al., 2001) were used to map to Manning's n values ($n = 0.220$ for reefs, Kennedy et al., 2012 and $n = 0.400$ for mangroves, Wolanski et al., 2013). These Manning's n values are used in SWAN to estimate the appropriate roughness length needed to calculate the spectral energy dissipation due to bottom friction (Dietrich et al., 2012; Madsen et al., 1989).

2.2. Experimental Design

Using the ADCIRC+SWAN+OWI configuration we simulate and describe the chronological history of Hurricanes Irma and Maria-induced coastal water levels and wave conditions in the PR and USVI region (section 3.1). In particular, we investigate relative contributions to coastal water levels from tides, inverted barometer response to atmospheric pressure, wind-driven surge, and wave-driven setup.

The following experiments were conducted to assess the forcing contributions:

1. Full ADCIRC+SWAN simulation. Forced with astronomical tides and both wind and atmospheric pressure fields.
2. Same as (1) but without astronomical tide forcing (no tidal potential, self-attraction and loading, or tidal boundary conditions).
3. Same as (2) but without wind wave coupling (no SWAN).
4. Same as (3) but without wind forcing (no surface stress).

The differences between successive experiments are used to determine an estimate of the contribution of each forcing. For example, the tidal contribution is calculated by taking the difference between (2) and (1). In this way it is possible to approximately account for the nonlinearities associated with the forcing combinations, because we use a top-down approach starting with the most complex setup and sequentially remove forcing components.

In addition to the above experiments using the ADCIRC+SWAN+OWI configuration, we investigate the sensitivity of the results to atmospheric forcing (section 3.2) and to the coastal flood circulation and wind wave model (section 3.3). In these sections coastal water levels simulated by ADCIRC are compared to observations at NOAA/NOS tide gauges and USGS rapid deployments (Figure 1 and Table 1). A mean sea level offset accounting for the effects of baroclinicity not represented in the calculation (Pringle et al., 2019) is used to postprocess modeled water levels for comparison to observations. This is calculated independently at each tide gauge based on the water level using the time period in between Hurricanes Irma and Maria and ranged between 0.10 and 0.14 m at an average of 0.11 m. Also, wave conditions simulated by SWAN are compared with observations made at the CARICOOS wave buoys. Error statistics used to assess performance at stations are as follows: mean error ($\bar{E}$), mean absolute error (*MAE*), mean normalized error (E_{NORM}), and the root-mean-square-error (*RMSE*; cf. Kerr, Martyr, et al.,2013). Errors are computed on both peak quantities and time histories.

The additional atmospheric forcings used are an operational dynamic hurricane model (HWRF), an operational dynamic synoptic model (CFSv2), and the Asymmetric Holland Parameteric Vortex (AHPV) model based on the Automated Tropical Cyclone Forecasting System (ATCF; https://www.nhc.noaa.gov/data) best-track data of the hurricanes (Table 2). HWRF should in theory simulate both hurricane intensity and synoptic meteorology adequately, but it is less constrained to observations than OWI. The global model, CFSv2, underestimates the hurricane intensity and overestimates its size, while AHPV cannot account for synoptic meteorology away from the hurricanes' radius of influence. Error statistics of the meteorology at the stations are also considered.

The other coastal flood circulation and wind wave model combination is SLOSH-FW (no tides, no advection, linear bottom friction, ocean depth limited to 100 m, Figure 3, first-generation wave model), which solves simplified versions of the underlying governing equations used in ADCIRC+SWAN (tides, advection, quadratic bottom friction, no ocean depth limiting, and third-generation wave model); refer to Table 2. The simplified wave model (FW) which has been newly developed to couple with SLOSH is an extension of the Schwab et al., 1984's (1984) first-generation model to allow more directional and frequency bins. Further, the experimental SLOSH-FW is simulated on a local domain consisting of 90-m to 1-km resolution structured curvilinear mesh (Figure 3) for SLOSH and a 1-km resolution structured grid for FW.

3. Results

3.1. Chronological History of Hurricane-Induced Water Level and Wave Fields

3.1.1. Hurricane Irma

On 30 August 2017, the beginnings of Hurricane Irma were detected by satellite off the west coast of Africa as a tropical depression. Within 30 hr, the eye of the storm had developed turning the storm into a hurricane which strengthened as it moved west southwest across the Atlantic toward the Antilles. Irma reached major

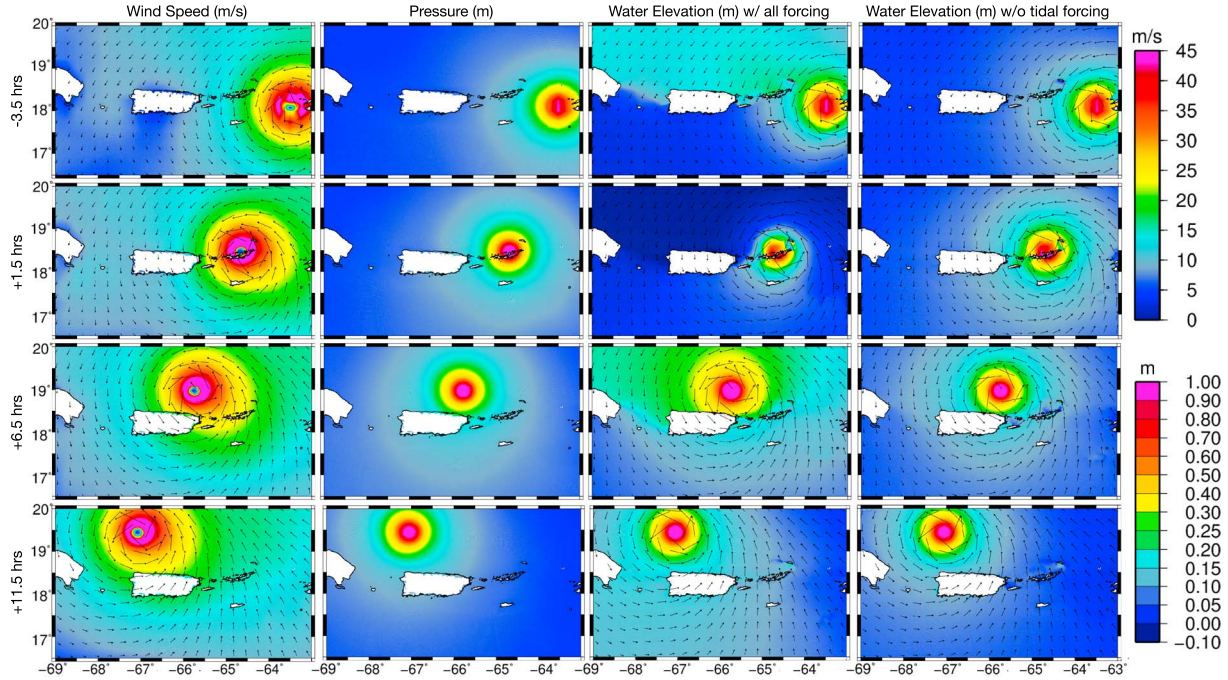

Figure 4. Wind speed (m/s; column 1), atmospheric pressure (m; column 2), water surface elevation (m; column 3), and water surface elevation without tides (m; column 4) for Hurricane Irma as computed by ADCIRC+SWAN+OWI. Atmospheric pressures are shown as pressure deficit from 1,013 mbar converted to meters of water. Select time snaps are shown with respect to landfall at Virgin Gorda, British Virgin Islands (6 September 2017, 1630 UTC) at −3.5, +1.5, +6.5, and +11.5 hr.

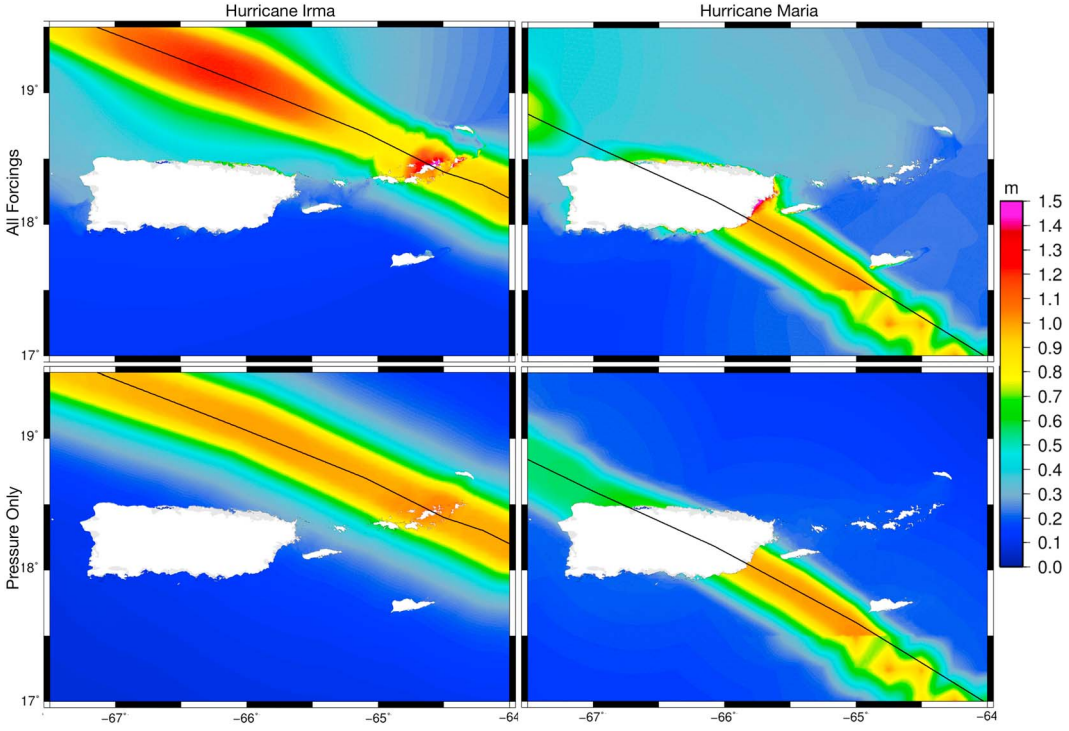

Figure 5. Maximum event water surface elevation for Hurricanes Irma and Maria from a full ADCIRC+SWAN coupled run (left olumn). Maximum event water surface elevation for Hurricanes Irma and Maria for a ADCIRC run forced only with atmospheric pressure (right column).

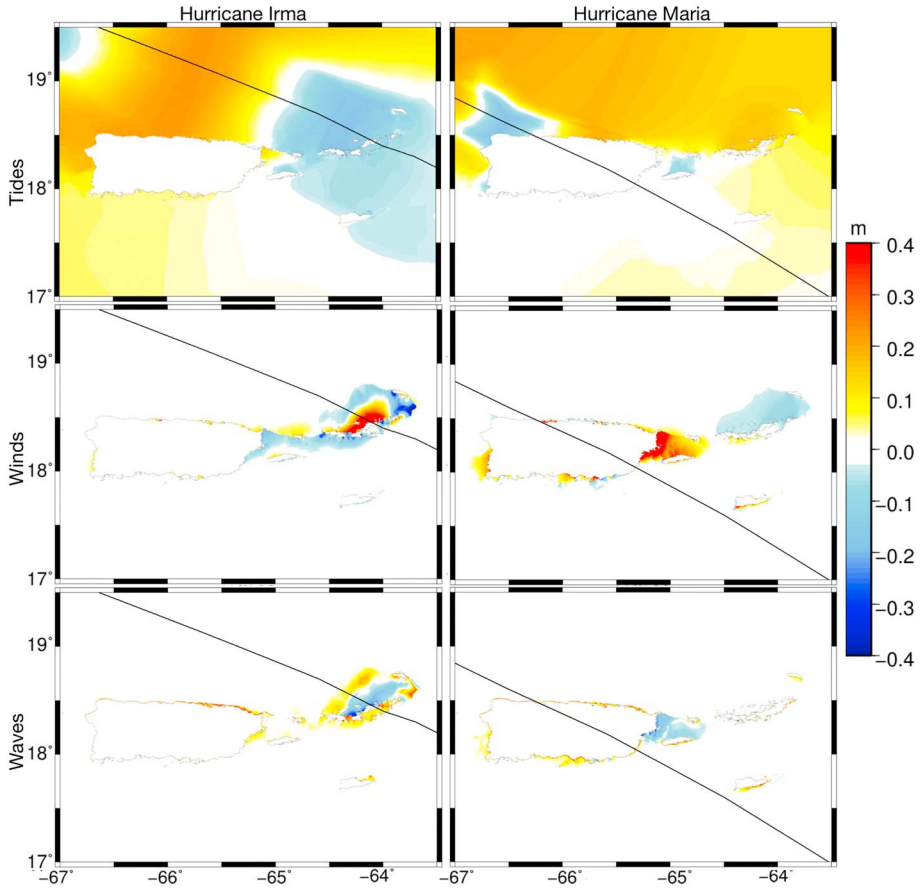

Figure 6. Tide, wind, and wave contributions to water levels as computed for Hurricanes Irma (left column) and Maria (right column) by the ADCIRC+SWAN+OWI model. Row 1 shows the effect on maximum event water surface elevation by tides. Row 2 shows the effect on maximum event water surface elevation by winds. Row 3 shows the effect on maximum event water surface elevation by waves.

hurricane status with a rapid rate of intensification matched by few storms. As the hurricane approached the Caribbean, it reached its maximum intensity on 5 September 1800 UTC, in the Atlantic Ocean approximately 70 miles east of Barbuda. First landfall was made by the storm at Barbuda on 6 September 0545 UTC with a minimum central pressure of 914 mbar and wind speeds reaching close to 80 m/s, and the second landfall was made less than 6 hr later at Saint Martin (Cangialosi et al., 2018) (Figure 4). The storm lost little to no intensity as it entered the area of interest for this study, making landfall at Virgin Gorda, British Virgin Islands on 6 September 1630 UTC. Both the British and U.S. Virgin Islands were subject to significant storm surge and waves as a result (Cangialosi et al., 2018).

Comparisons of the atmospheric pressure deficit (in meters of water) to time snaps of the water elevation response without tidal forcing (Figure 4), and the maximum storm event water level with all forcings and with pressure forcing only (Figure 5) suggests that the majority of storm surge affecting the Virgin Islands was driven by the inverted barometer response to the central minimum storm pressure. This pressure-driven response accounted for 0.8 to 1 m of water level increase in the vicinity of the storm track and approximately 30 cm along the northern coasts of PR.

The contribution of tides to water levels is highlighted in Figures 4 and 6, indicating that the stronger Atlantic tides impact total water level there more than in the Caribbean. Tides lowered maximum water levels in the Virgin Islands at the time of peak surge (Figure 6). The passing of Irma by PR coincided with a high tide along most of the Atlantic facing coast of the island, increasing storm event maximum total water levels. This can be seen in Figure 4 in the water surface elevation fields comparing the simulations with and without tidal forcing at +6.5 hr after landfall and in the tidal contribution to maximum water levels in Figure 6. The

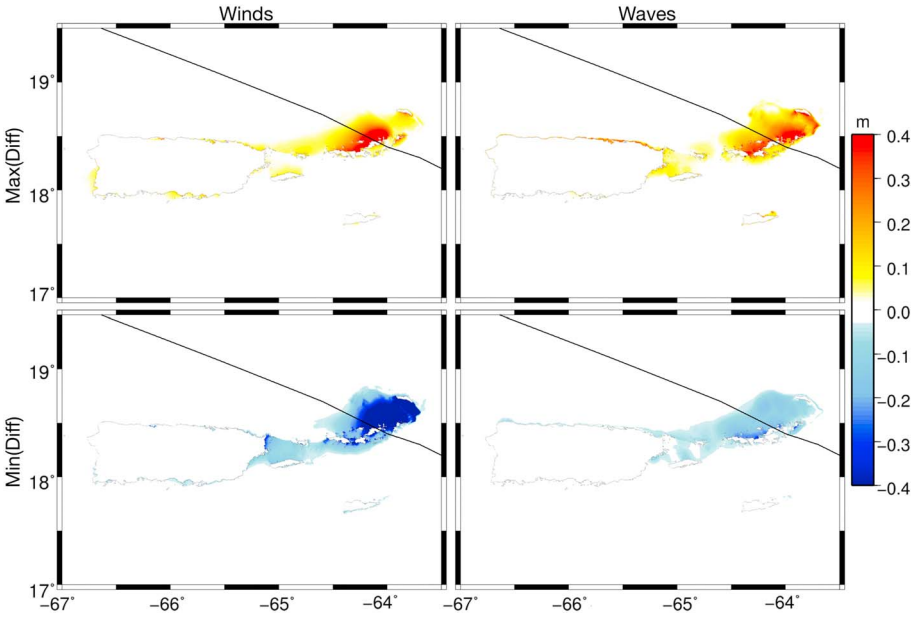

Figure 7. Maximum positive and negative contributions by (left column) winds and (right column) wave effects to water levels as computed for Hurricane Irma by the ADCIRC+SWAN+OWI model. Row 1 shows the maximum effect on event water surface elevation by winds and waves. Row 2 shows the minimum effect on event water surface elevation by winds and waves. This figure supplements the effect of winds and waves on the maximum water levels shown in Figure 6 of the main paper.

impact of tides on total water levels was up to 0.25 m on the Atlantic side of the islands and less than 0.10 m on the Caribbean side.

The effect of wind-driven surge was comparatively weak overall, only contributing to maximum water levels positively on the Atlantic facing coast of the Virgin Islands (Figures 6 and 7) as the incoming Category 5 hurricane winds from the storm blew over the shallow bathymetry on the shelf there. It is noted that the shelf is wider on the Atlantic side of the Virgin Islands than the Caribbean side (Figure 3). A strong drawdown occurred as the storm passed the Virgin Islands and blew water away from the islands across the shelf and into the Atlantic (Figure 7). A negative contribution also can be observed east of PR due to strong winds pushing water away from the island off the shallow shelf which is separated from the Atlantic by the reef system to the north. On the north coast of PR a small positive effect was also observed. As the storm moved outside of the study area to the west, strong winds induced a small rise in water levels on the southwest coast of PR. Maximum positive and negative impact of winds was at least 0.30 m in the Virgin Islands and less than 0.15 m on the coasts of PR.

Wave-induced setup occurred both on the Atlantic and Caribbean facing coasts of the Virgin Islands (Figures 6 and 7). This was caused by waves directed onto the adjacent shelves and shores both prior to and after landfall (Figure 8) inducing strong wave forces. We estimate that waves from the Atlantic Ocean induced a strong setup of at least 0.35 m on the northern shelf and coasts of the USVI prior to the storm passing the Virgin Islands (Figures 6 and 7). At the time of passage of the storm, winds were directed from the south and waves impinged on the islands creating a smaller setup of up to 0.15 m on the Caribbean facing side. At this time rapid wave growth over the shallow shelf in the direction of the Atlantic on the northern side of the islands caused a wave set down of up to 0.20 m (Figures 6 and 7). As the storm moved to the west, the hurricane generated waves with significant wave heights exceeding 10 m, propagating in the southeast direction, partially headed toward the PR coast. The breaking of these waves on the northeast of the island led to the development of a strong wave force directed perpendicularly to the coast. The resulting up to 0.30 m setup was narrowly focused at the north coast of PR (Figures 6 and 7).

3.1.2. Hurricane Maria

Less than 3 weeks after Hurricane Irma formed, a tropical depression appeared approximately 1,000 km to the east of Barbados on 16 September 1200 UTC. By 17 September 1800 UTC, the tropical depression had moved westward and developed into a hurricane. As the hurricane moved across the Atlantic, warm sea

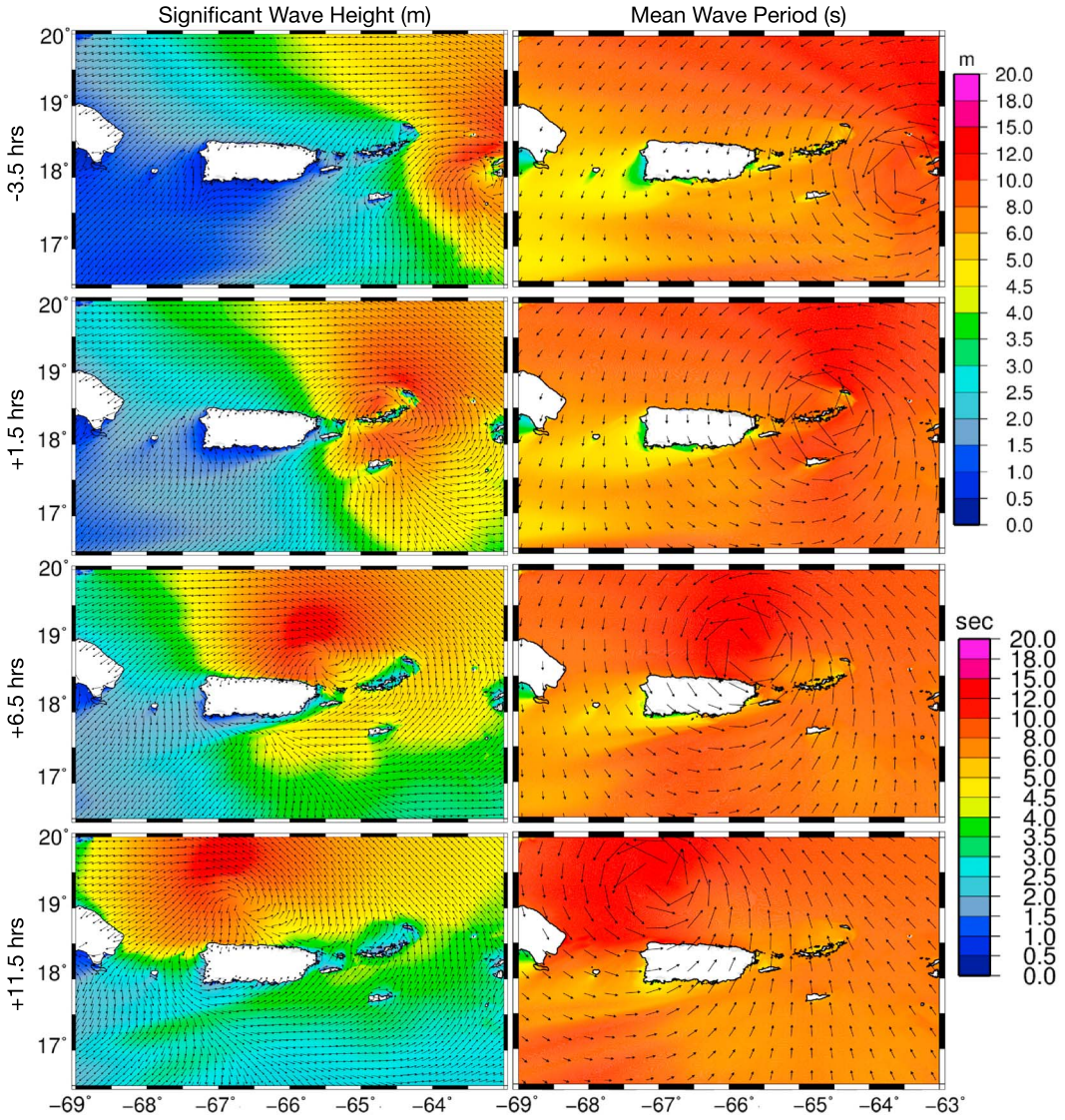

Figure 8. ADCIRC+SWAN output significant wave height (m) with vectors representing wave direction (left column) and mean wave period (s) with vectors representing wind speed (right column) at select times with respect to landfall for Hurricane Irma at the British Virgin Islands.

surface temperatures led to strong intensification and wind speeds greater than 75 m/s as the storm made initial landfall on Dominica in the Antilles. The mountainous terrain of Dominica weakened the storm slightly, but it quickly intensified as it headed northwest toward the island of PR. The hurricane weakened somewhat before landfall, but made direct landfall at Yabucoa Harbor in the southeast corner of PR on 20 September 1015 UTC, still with wind speeds approaching 70 m/s and a minimum low pressure nearing 920 mbar. Hurricane Maria traveled across almost the entirety of the island, exiting the landmass at Arecibo on 20 September 1800 UTC having weakened but still with wind speeds exceeding 45 m/s (Pasch et al., 2018).

The model results indicate that the largest primarily pressure-driven storm surge was approximately 1.5 m at its maximum and developed along the eastern Puerto Rican coastline (Figures 5 and 9). Almost 1 m of the storm surge developed at Yabucoa Harbor which can be directly attributed to the storm's minimum central pressure. Despite the storm weakening over PR and the associated increase in the central pressure, a significant pressure-driven increase in water levels of around 0.8 m was observed and modeled on the northwestern coast of the island as well.

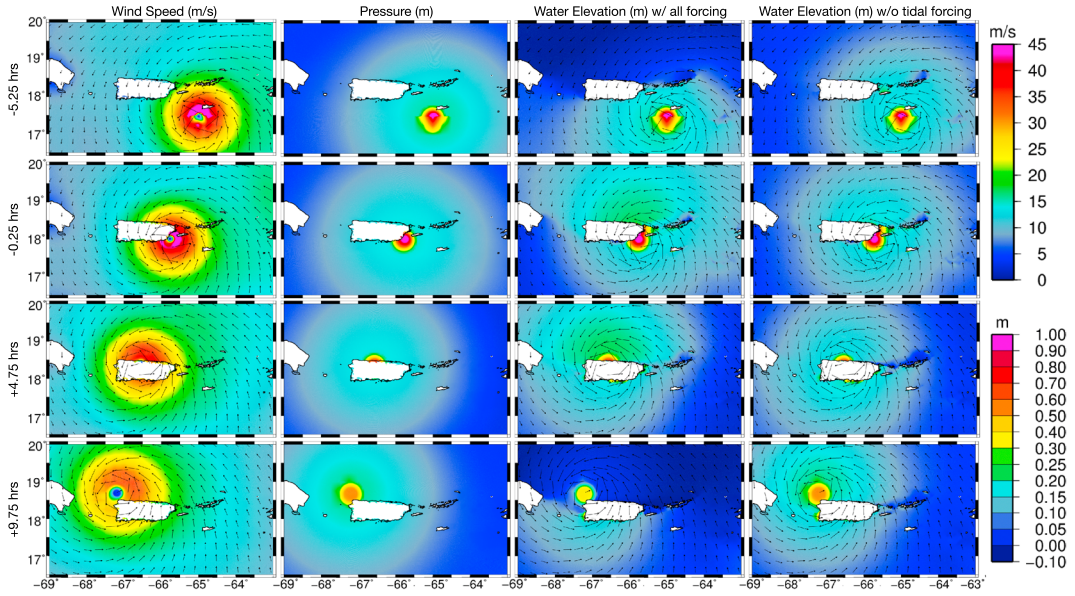

Figure 9. Wind speed (m/s; column 1), atmospheric pressure (m; column 2), water surface elevation (m; column 3), and water surface elevation without tides (m; Column 4) for Hurricane Maria as computed by ADCIRC+SWAN. Atmospheric pressures are shown as pressure deficit from 1,013 mbar converted to meters of water. Select time snaps are shown with respect to landfall at Yabucoa (20 September 2017 1015 UTC) at −5.25, −0.25, +4.75, and +9.75 hr.

Figures 6 and 9 highlight that tides had little to no effect on the maximum water levels at the point of landfall at Yabucoa. However, along the northeastern shore of PR, a high tide occurred as the storm crossed over the island. By the time Maria reached the northwestern corner of the island and made its way into the Atlantic at Arecibo, the tides worked to decrease the total water level. The tidal contribution to total coastal water levels was proportionally much smaller during Hurricane Maria due to the much larger overall water level increases.

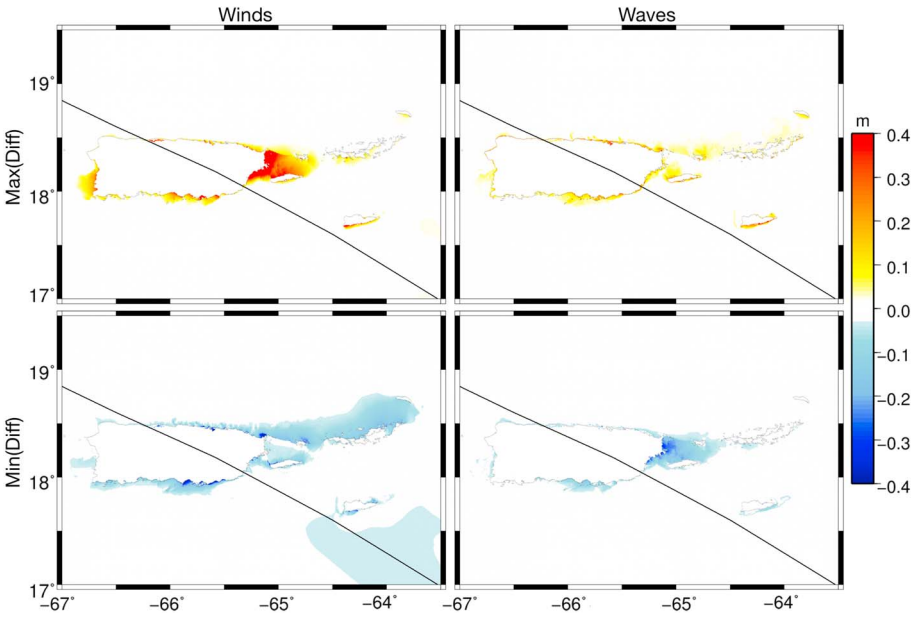

Figure 10. Maximum positive and negative contributions by (left column) winds and (right column) wave effects to water levels as computed for Hurricane Maria by the ADCIRC+SWAN+OWI model. Row 1 shows the maximum effect on event water surface elevation by winds and waves. Row 2 shows the minimum effect on event water surface elevation by winds and waves. This figure supplements the effect of winds and waves on the maximum water levels shown in Figure 6 of the main paper.

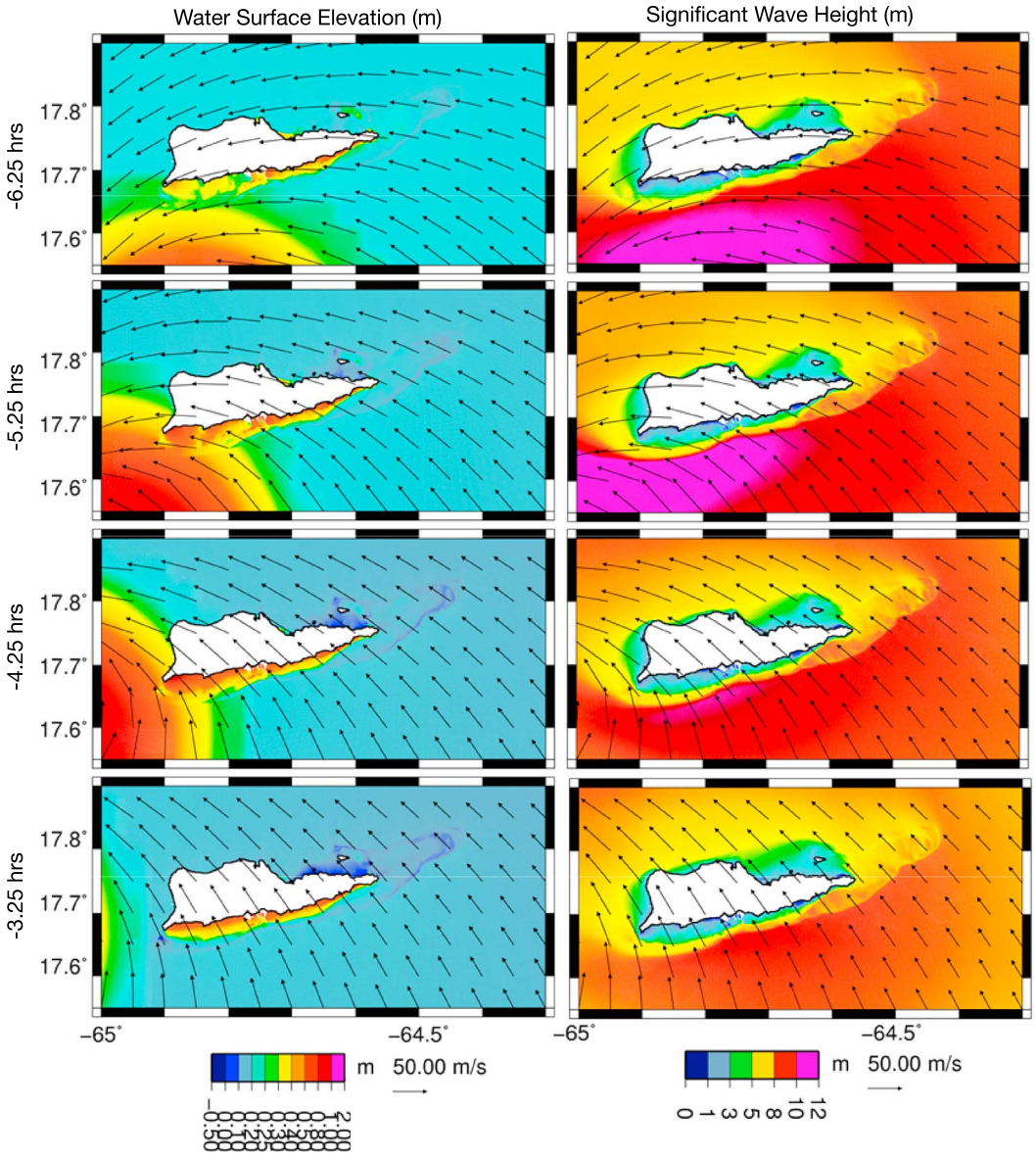

Figure 11. Water surface elevation (left column) and significant wave height (right column) as Hurricane Maria approached and moved past the waters of St. Croix. Results from ADCIRC+SWAN using PRVI15 mesh and OWI pressure and wind fields are shown. Vectors show wind speed.

Figures 6 and 10 suggest that the wind-generated contribution to the total maximum event water level along the south shore of St. Croix was approximately 0.3 m. Strong winds on the right side of the storm led to a wind-driven surge at St. Croix to the southeast of Puerto Rico approximately 5 hr before landfall (Figure 9 with details in Figure 11). As Maria passed St. Croix (Figure 11, third and fourth snapshots), the winds oriented perpendicular to the coast generated surge against the island. As Maria approached the shallow shelf east of PR, the effects of bathymetry, topographic obstacles, and geometry became apparent. Water level increases driven by strong easterly winds occurred on the northeast side of PR and the northwestern corner of Vieques (where there is a large sand bank), while Maria was still offshore in deep waters (see first snapshot of Figure 12). Until Maria made landfall, storm surge increased on the northern east coast of PR. Furthermore, the large reef system to the east off the northeastern corner of PR has a blocking effect causing surge to pile up in this area despite the winds blowing offshore (last two snapshots in Figure 12). The largest wind-driven contributions to surge along the eastern coastline of PR were up to 1 m and focused to the north of the storm track (Figures 6 and 10). This large contribution can be attributed to the extensive

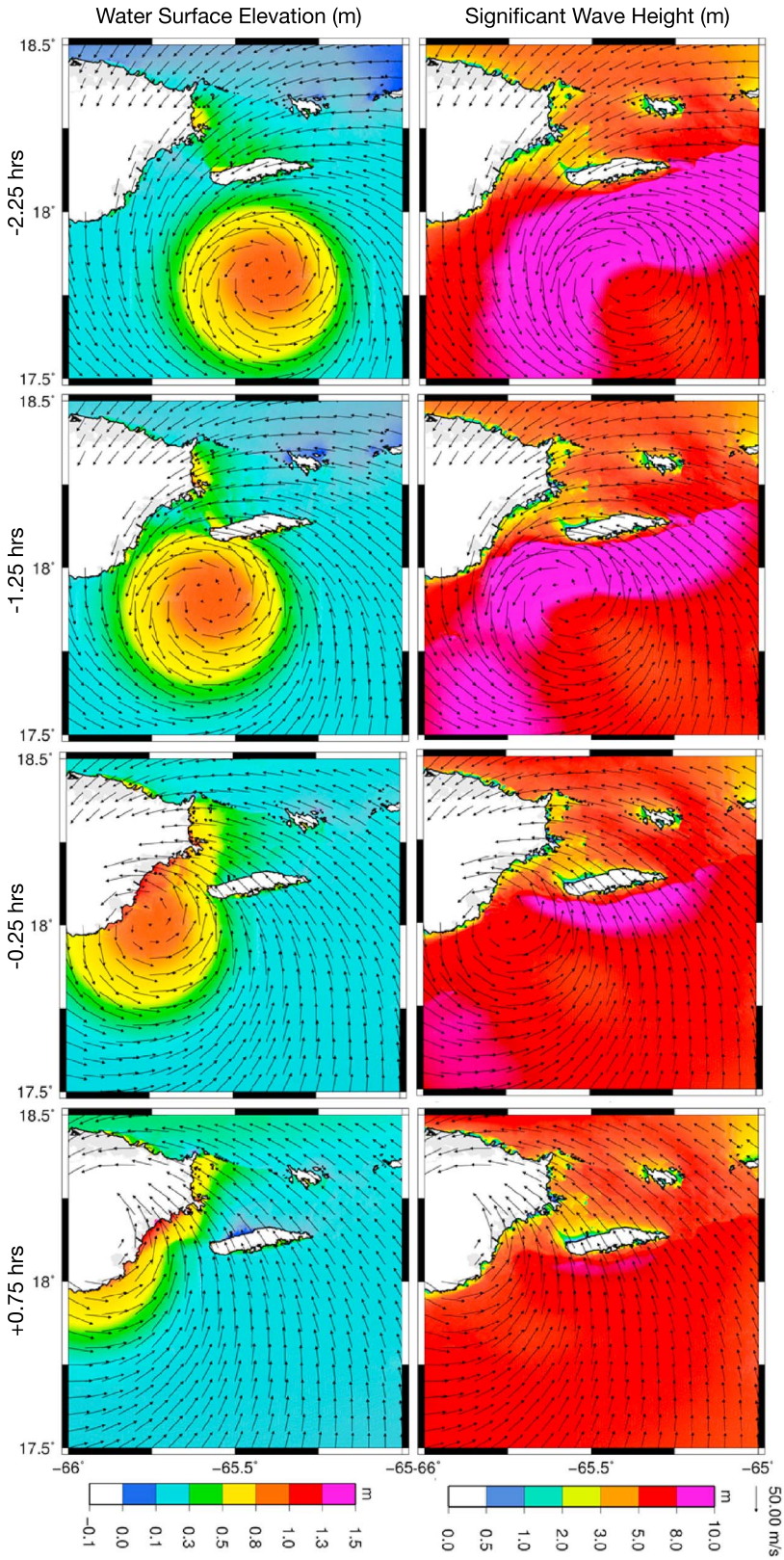

Figure 12. Water surface elevation (left column) and significant wave height (right column) as Hurricane Maria approached and made landfall over the east waters of Puerto Rico. Results from ADCIRC+SWAN using PRVI15 mesh and OWI pressure and wind fields are shown. Vectors show wind speed.

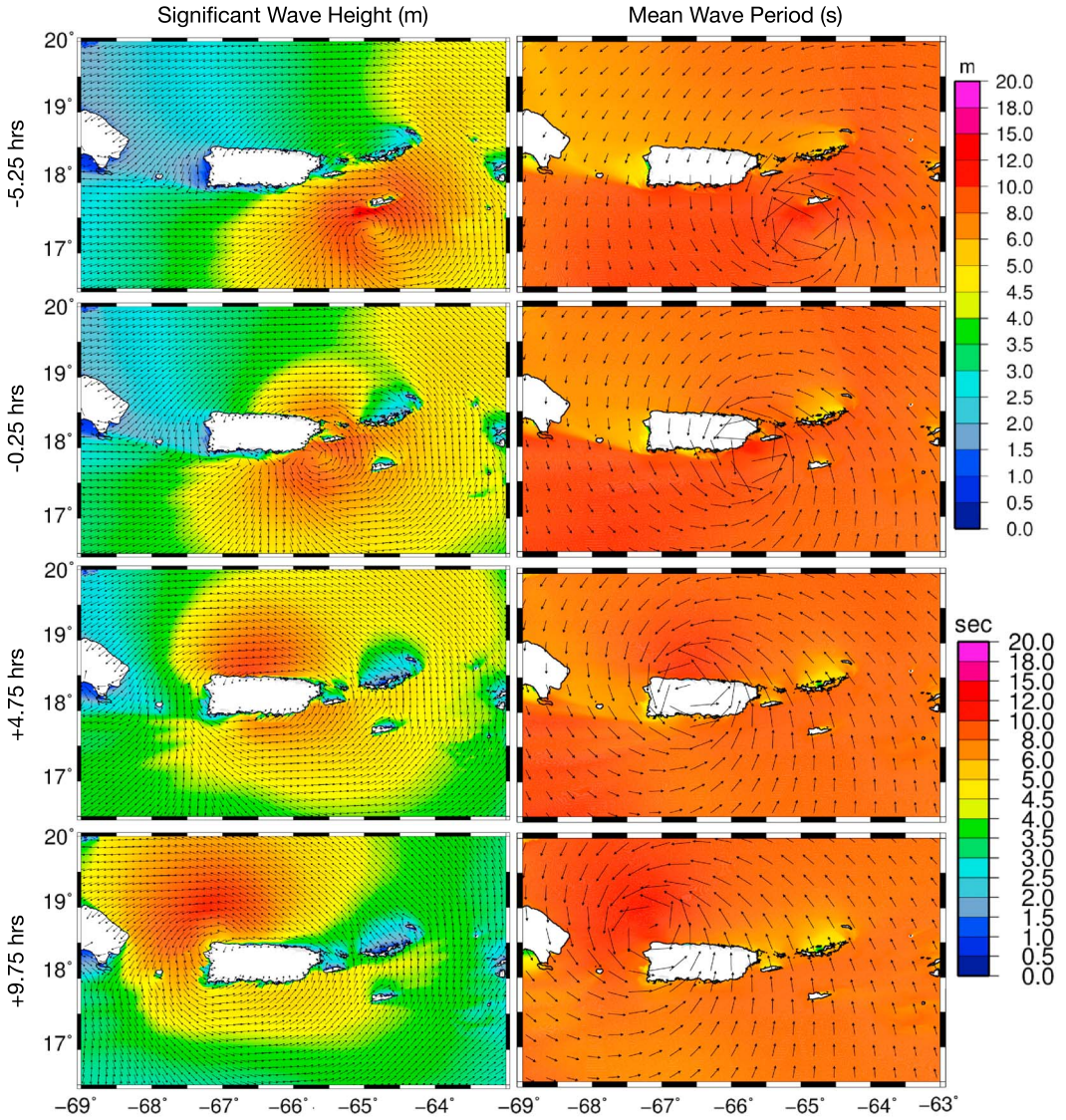

Figure 13. ADCIRC+SWAN output significant wave height (m) with vectors representing wave direction (left column) and mean wave period (s) with vectors representing wind speed (right column) at select times with respect to landfall for Hurricane Maria at Yabucoa.

shallow shelf in the region which extends over 100 km to the east of PR and is highlighted in Figure 3. The cyclonic nature of the storm also directed wind-driven surge toward the northern, western, and southern coasts as the storm crossed the island (see +9.75 hr after landfall in Figures 6, 9, and 10), which continued as the storm progressed further to the northwest and out of the study region. This wind-driven surge is up to 0.3 m and the area where these contributions are the largest correspond to the coasts with somewhat wider shelves in the region. However, only the eastern shelf extends out beyond 100 km; the shelves along northern coasts extend only a few kilometers offshore, while the western and southern shelves extend as far as 25 km in places. It is clear that the wind-driven component of storm surge is strongly dependent on shelf width and bathymetric profile.

Wave-driven effects were an important factor in a number of areas within the study region for Hurricane Maria. At St. Croix the large waves generated by the storm broke on the shallow bathymetry of the Caribbean facing the side of the island (Figure 13, detailed in Figure 11). In the first two snapshots the winds are blowing parallel to southern coast of St. Croix, while wave breaking reduces the wave height from >12 m to 1–3 m over a distance of approximately 7 km from the coast to the shelf break. The wave breaking generated enough radiation stress to sustain a wave-driven surge component of over 0.3 m over the shelf (Figures 6

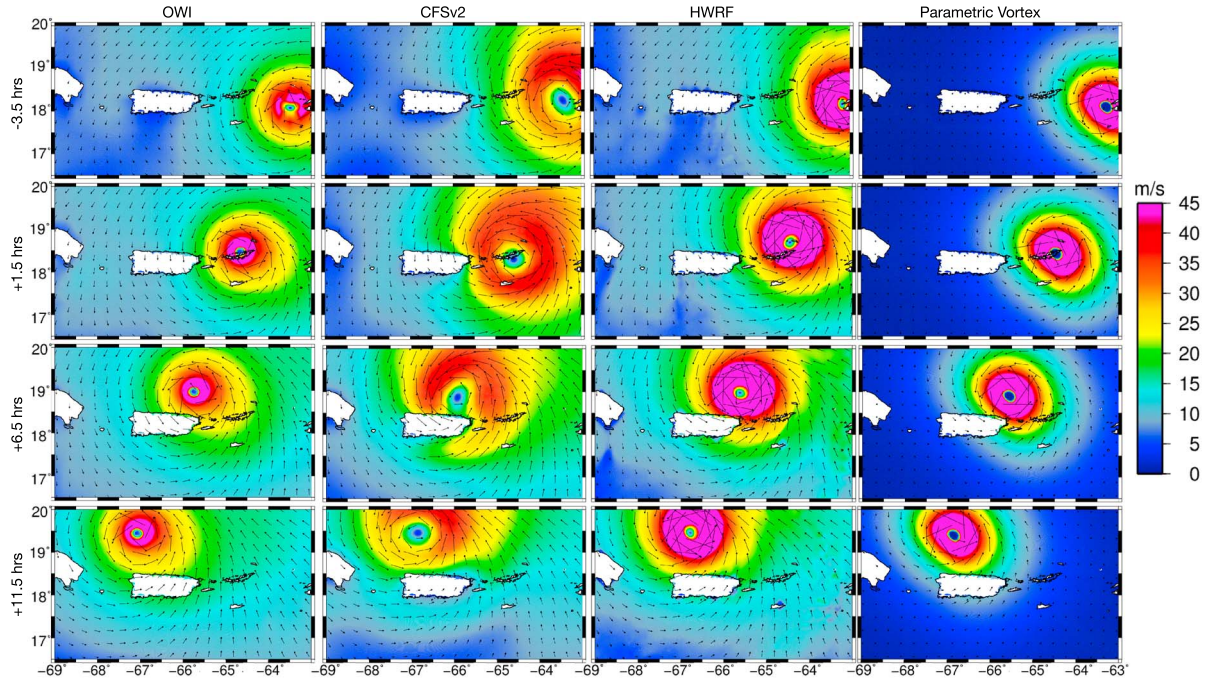

Figure 14. Wind speed (m/s) from the OWI model (column 1), CFSv2 model (column 2), HWRF model (column 3), and AHPV model (column 4) for Hurricane Irma at select times with respect to landfall at the British Virgin Islands.

and 10). This illustrates how the island shelf can intensify the storm surge even when there is no direct landfall, through increased radiation stress from the breaking of large waves. A similar but smaller wave setup effect (~0.1 m) occurred at the southeast facing side of Vieques (Figures 6 and 10). Interestingly, to the northwest of Vieques over the shelf, a minor wave-induced set down on the order of 0.2 m in maximum water levels is observed at the time of maximum surge (Figures 6 and 10). Figure 12 shows the effect of the reefs, banks, and the steep slopes of the area. Notice how the highest waves with heights of 10 m or more are limited to the deep waters and as soon as the hurricane wave field interacted with the shelf, wave heights

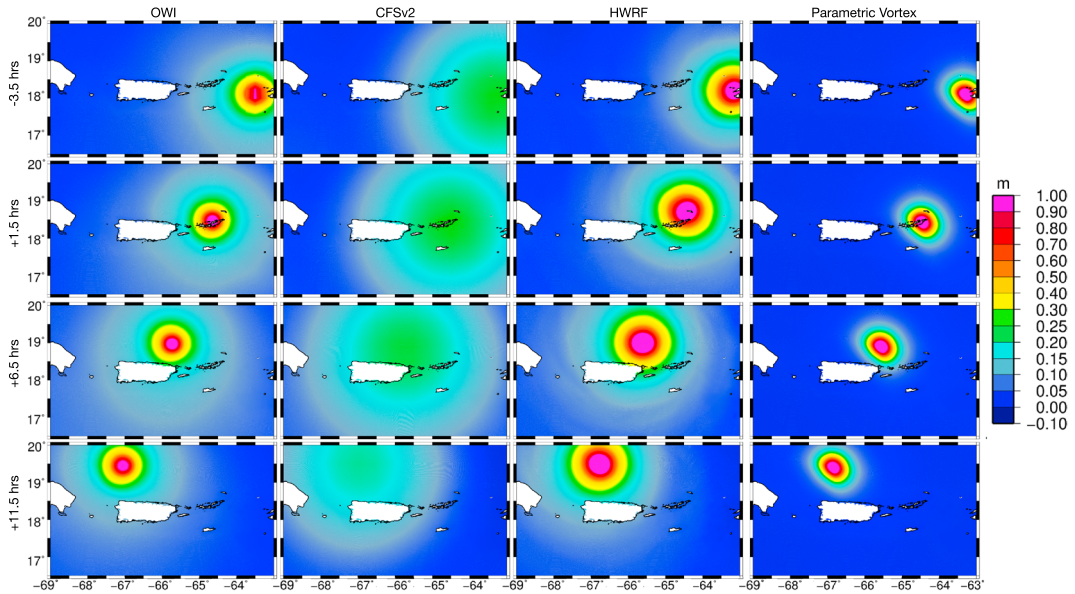

Figure 15. Atmospheric pressure deficit (m of water) from the OWI model (column 1), CFSv2 model (column 2), HWRF model (column 3), and AHPV model (column 4) for Hurricane Irma at select times with respect to landfall for Hurricane Irma at the British Virgin Islands.

Table 3
Hurricane Irma Atmospheric Forcing Errors

Irma forcing	Forcing	$\bar{E}$	*MAE*	E_{NORM}	*RMSE*	*N*
Min pressure timing (hr)	AHPV	1.86	1.86			10
	CFS	0.67	1.09			
	OWI	0.02	0.44			
	HWRF	1.57	2.01			
Min pressure error (m)	AHPV	−0.11	0.12	0.69		10
	CFS	−0.02	0.09	0.37		
	OWI	0.01	0.02	0.07		
	HWRF	0.01	0.04	0.12		
Pressure (m)	AHPV	−0.072	0.073		0.082	11
	CFS	0.031	0.046		0.056	
	OWI	0.004	0.010		0.013	
	HWRF	0.004	0.018		0.027	
Windspeed (m/s)	AHPV	1.18	4.96		6.1	11
	CFS	6.88	7.29		8.55	
	OWI	7.25	7.39		8.29	
	HWRF	6.09	6.65		7.9	

Note. Minimum atmospheric pressure error, pressure time series errors, and wind speed time series errors are shown. Units are as denoted except for E_{NORM}. *N* represents sample size. Lowest errors are underlined.

abruptly decreased to 5–8 m, and then down to 1–3 m, all in a short distance of about 4–5 km. Over the shelf, waves grew locally, resulting in the set down seen at the time of maximum surge. On the shelf, the various reef and bank features, along with the short fetch inside the shelf, limited the wave heights to a maximum of about 6 m, progressively decreasing in heights to about 1–3 m along the coastline, behind the extensive line of natural barriers in this area. As such, the shelf-reef system as a whole acts to significantly dissipate the hurricane wave field and limit the extent of the coastal hazards and damages on the east coast of PR. Waves generated by the storm while it was over the island were directed toward the northern coast of PR (shown in Figure 13), and their breaking led to wave-induced setup on the order of 0.3 m there (Figures 6 and 10).

3.2. Atmospheric Forcing Comparison

3.2.1. Hurricane Irma

Generally, the representation of Hurricane Irma differs significantly from one meteorological model to the next. As seen in Figures 14 and 15, before landfall, the OWI representation of the storm is aliased due to low grid resolution outside of the high-resolution inset to the east of the Virgin Islands. This improves as the storm moves into the high-resolution inset near areas of interest. OWI has the lowest of all error metrics related to the minimum atmospheric pressure ($\bar{E} = 0.01$ m and $MAE = 0.02$ m, Table 3). Additionally, the time series comparisons of atmospheric pressure show that OWI has the lowest *MAE* (0.010 m) and *RMSE* (0.013 m). The ADCIRC+SWAN computed HWM magnitude and timing errors for OWI are also among the best performing, in addition to wave property time series analysis with the lowest *MAE* and *RMSE* for both significant wave height and mean wave period (Table 4).

The CFSv2 model produces a diffuse and asymmetrical representation of the wind field with a relatively weak central pressure compared to the other atmospheric forcings (Figures 14 and 15). These properties lead to significant differences in the directionality of the winds as the storm passes north of PR, adversely affecting ADCIRC+SWAN-modeled coastal water levels. For example, shore perpendicular winds found in the CFSv2 fields lead to larger waves (see the SWAN wave field at the PR2 station in Figure 16) and wave-induced setup along the north coast of PR, compared to the OWI and AHPV runs in which the winds are more shore parallel. This results in an overprediction of the water surface elevation at San Juan and Arecibo (Figure 17) despite lower maximum wind speeds and a smaller pressure deficit than the other forcing products. Overall, the CFSv2 product performs well at stations where there was no significant storm surge and has the lowest peak water level *MAE* of 0.13. CFSv2 also had the lowest overall water level time series $\bar{E}$, *MAE*, and *RMSE*

Table 4
Hurricane Irma Model Response Errors for All the ADCIRC+SWAN PRVI15 Model With All Atmospheric Forcings and the SLOSH-FW Model Forced With OWI and With ADCIRC Tides Added

Irma response	Simulation	$\bar{E}$	*MAE*	E_{NORM}	*RMSE*	*N*
HWM timing (hours)	AHPV	−6.7	7.5			10
	CFS	−1.75	2.86			
	OWI	−1.57	2.63			
	HWRF	−1.74	2.72			
	SLOSH-FW	−1.89	3.59			
HWM (m)	AHPV	−0.12	0.27	0.76		10
	CFS	0.07	0.13	0.51		
	OWI	−0.03	0.19	0.62		
	HWRF	0.08	0.21	0.69		
	SLOSH-FW	−0.08	0.13	0.23		
WSE (m)	AHPV	−0.11	0.14		0.12	11
	CFS	0	0.06		0.06	
	OWI	−0.04	0.07		0.07	
	HWRF	−0.03	0.08		0.08	
	SLOSH-FW	−0.04	0.09		0.09	
SWH (m)	AHPV	−0.7	0.83		0.92	4
	CFS	−0.11	0.43		0.62	
	OWI	−0.14	0.32		0.45	
	HWRF	−0.14	0.56		0.75	
	SLOSH-FW	0.14	0.95		1.18	
Wave direction (deg)	AHPV		37.51		53.50	4
	CFS		24.76		40.89	
	OWI		25.97		41.48	
	HWRF		36.53		53.84	
	SLOSH-FW		50.47		65.94	
Mean wave period (s)	AHPV	5.73	7.85		9.02	4
	CFS	−1.73	2.76		3.8	
	OWI	−1.77	2.15		3.27	
	HWRF	−2.7	3.9		5.01	
	SLOSH-FW					

Note. Peak surge (HWM) error, water surface elevation time series, and wave property (significant wave height, SWH, wave direction, and mean wave period) time series are shown. Units are as denoted except for E_{NORM}. *N* represents sample size. Lowest errors are underlined.

for Hurricane Irma, although OWI and HWRF produced similarly low errors. This is related to the overall excellent wind and pressure properties away from the core of the storm.

The HWRF model produces the strongest and highest energy representation of the storm, generally overestimating the central pressure deficit and wind speeds (Figure S1 in the supporting information and Table 3). The size of the storm is similar to the diffuse CFSv2 representation, but the wind speeds are faster and the pressure deficit is larger than the OWI product (Figures 14 and 15). At water level stations with significant storm surge, the HWRF-driven ADCIRC+SWAN surge is stronger than that with the other wind forcings. The peak surge using HWRF is overestimated by 0.08 m on average ($\bar{E}$).

The AHPV model produces an asymmetric storm which has a stronger but also narrower wind and pressure field than the OWI product. On the north side of the island, where ADCIRC+SWAN surges are primarily driven by waves and winds, the AHPV model performs comparably to the OWI winds. However, because there is no background atmospheric field outside of the storm core the water levels are underpredicted on the southern regions far away from the storm track. Thus, the AHPV results in the greatest underestimate

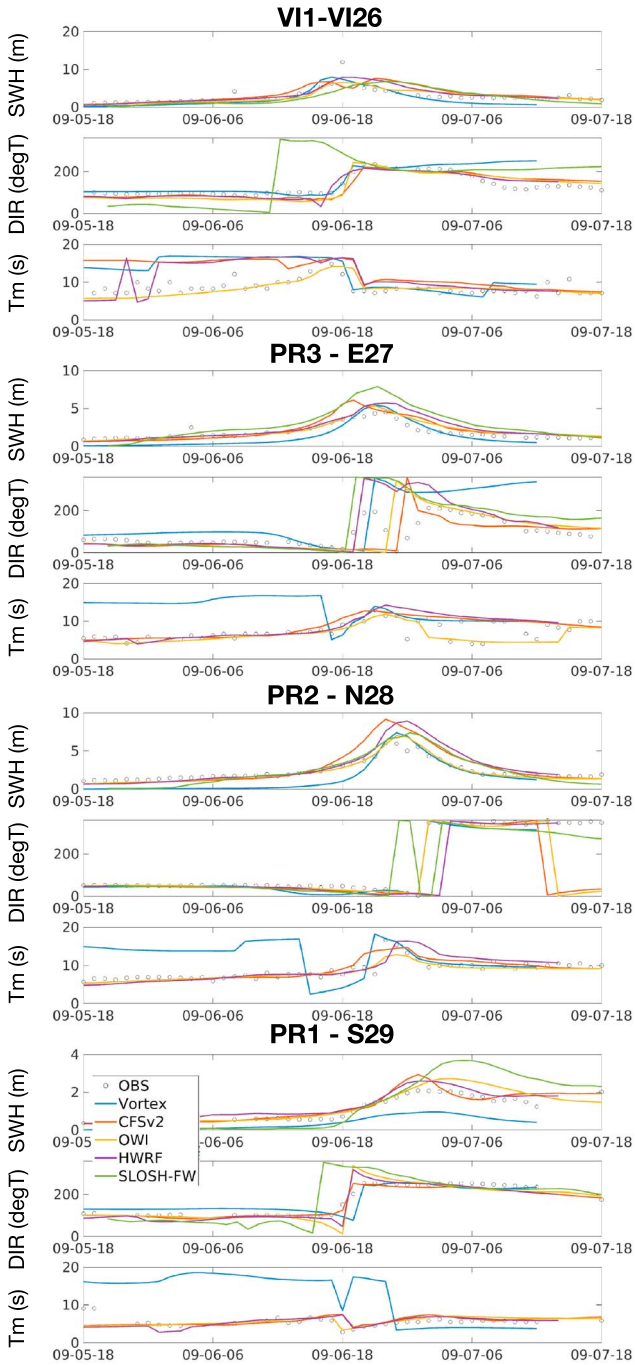

Figure 16. Modeled ADCIRC+SWAN (forced by all wind products) and SLOSH-FW (forced by OWI) significant wave height and direction time series compared to observed data at a CARICOOS wave gauges during Hurricane Irma. Mean wave period comparisons are shown for the ADCIRC+SWAN runs. PR = Puerto Rico.

in the average HWM error ($\bar{E} = -0.12$ m), and the largest relative HWM error averaged for all regions ($E_{NORM} = 0.76$). In addition, the time series errors in the water surface elevation, significant wave height, and mean wave period are largest for the AHPV forcing (Table 4).

3.2.2. Hurricane Maria

The general characteristics of Hurricane Maria (Figure 18 and 19) in each of the atmospheric forcing models are comparable to the corresponding product's representation of Hurricane Irma: the OWI product provides the most reasonable estimate of the storm characteristics as well as background atmospheric conditions

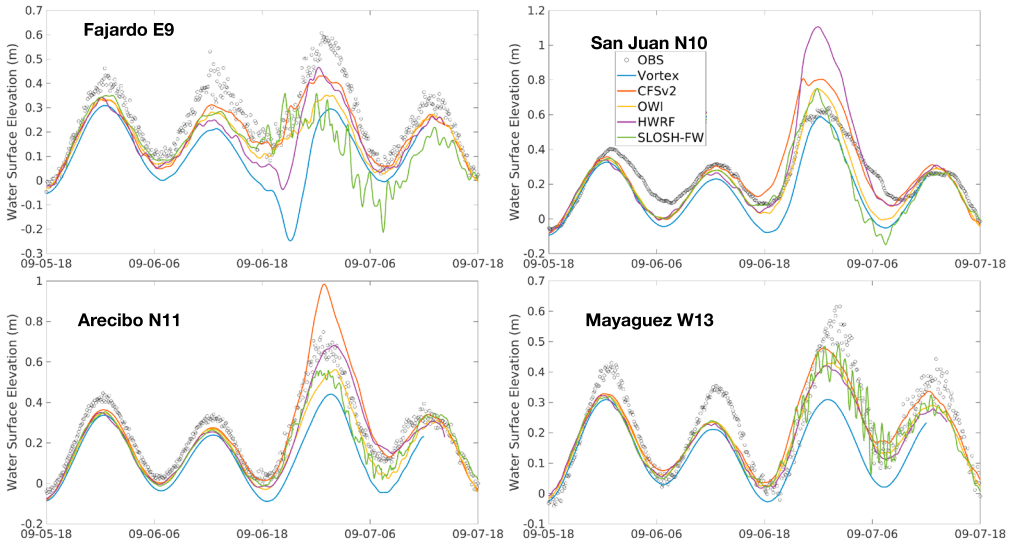

Figure 17. Modeled ADCIRC+SWAN (forced by all wind products) and SLOSH-FW (forced by OWI and with ADCIRC-computed tides added) water surface elevation time series compared to observed data at a selection of NOAA/NOS water level gauges during Hurricane Irma.

away from the storm's radius, the CFSv2 model's representation of the storm is too diffuse and the structure of pressure field and minimum central pressure is not captured, the HWRF overestimates the storm pressure deficit and wind speeds, and the AHPV model most closely resembles the OWI product in terms of the wind speed and pressure at or near the center of the storm (Figure S2). The minimum atmospheric pressure and time series atmospheric pressure errors are generally larger for Hurricane Maria compared to Hurricane Irma across all of the atmospheric forcings. An exception is the AHPV model which performs better for Hurricane Maria due to the storm track passing more closely to the observations stations compared to Hurricane Irma. Like Hurricane Irma, the overall atmospheric pressure error metrics are lowest for the OWI product (Table 5).

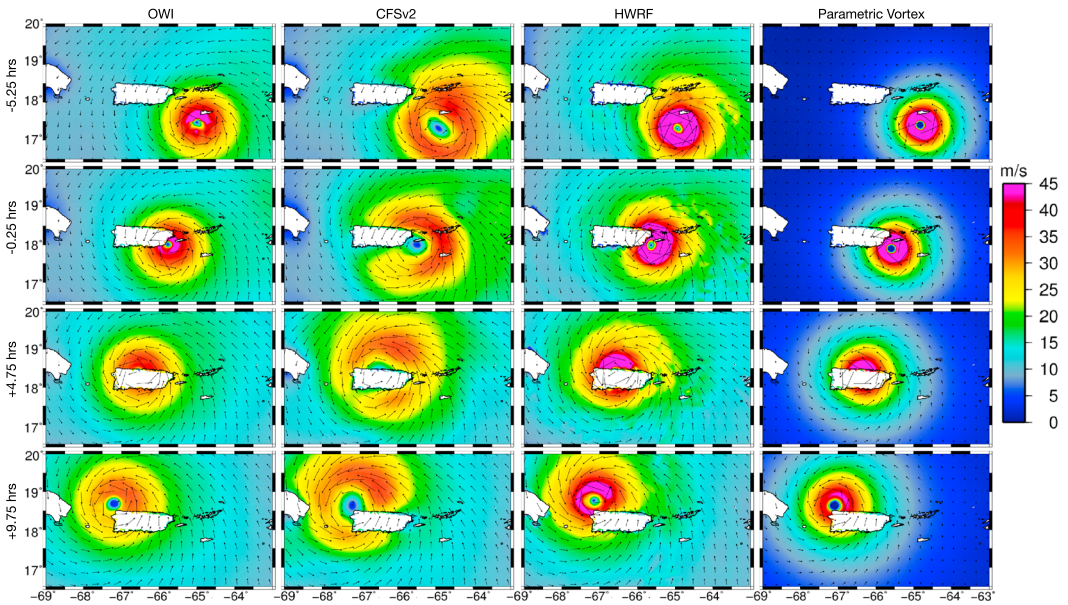

Figure 18. Wind speed (m/s) from the OWI model (column 1), CFSv2 model (Column 2), HWRF model (column 3), and AHPV model (column 4) for Hurricane Maria at select times with respect to landfall at Yabucoa Harbor, Puerto Rico.

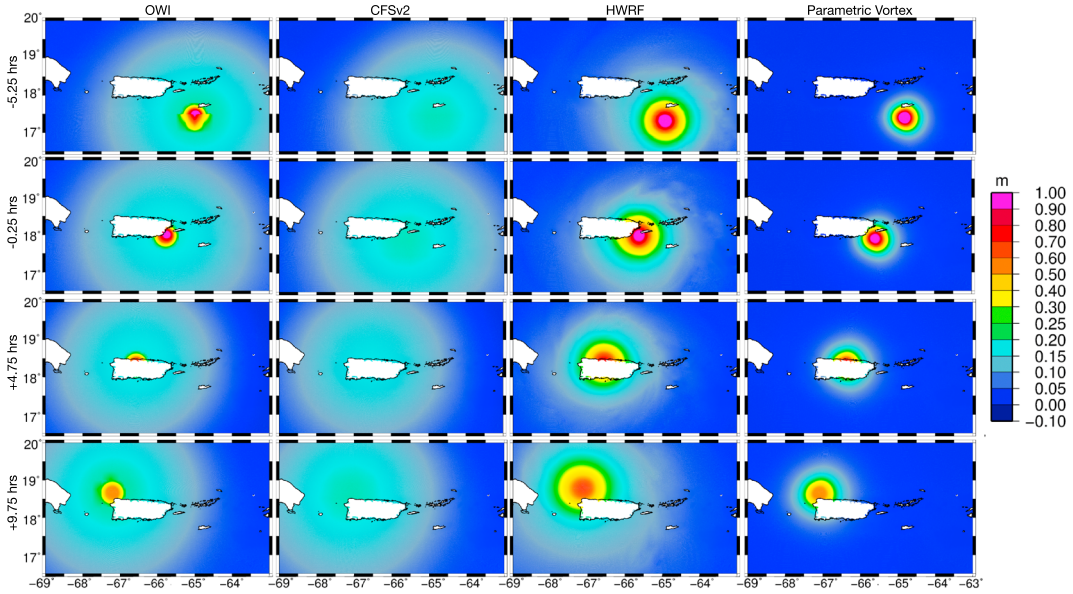

Figure 19. Atmospheric pressure deficit (meters of water) from the OWI model (column 1), CFSv2 model (column 2), HWRF model (column 3), and AHPV model (column 4) for Hurricane Maria at select times with respect to landfall at Yabucoa Harbor, Puerto Rico.

The average normalized ADCIRC+SWAN HWM errors are smallest for OWI (E_{NORM} = 0.26), followed the AHPV model (E_{NORM} = 0.35), CFSv2 (E_{NORM} = 0.42), and lastly HWRF (E_{NORM} = 0.53). The CFSv2 forced model significantly underrepresents the peak surge on average, but this is particularly clear at Yabucoa (Figure 20) where the pressure-driven surge dominates overall water levels. Underprediction is also seen in the CFSv2 simulation to the north of Yabucoa at Ceiba where wind-driven surge was important and the CFSv2 wind speeds over the shelf are significantly weaker than the rest of the forcing suite. The OWI time series *MAE* and *RMSE* is also smallest for water surface elevation, showing the level of overall

Table 5
Hurricane Maria Atmospheric Forcing Errors

Maria forcing	Forcing	$\bar{E}$	*MAE*	E_{NORM}	*RMSE*	*N*
Min pressure timing (hr)	AHPV	0.44	0.94			16
	CFS	1.66	3.52			
	OWI	0.37	1.06			
	HWRF	1.79	1.87			
Min pressure error (m)	Vortex	−0.07	0.15	0.35		16
	CFS	−0.31	0.32	0.58		
	OWI	−0.11	0.15	0.32		
	HWRF	0.05	0.15	0.33		
Pressure (m)	AHPV	−0.096	0.103		0.113	21
	CFS	−0.039	0.066		0.101	
	OWI	−0.021	0.055		0.076	
	HWRF	−0.008	0.056		0.081	
Windspeed (m/s)	AHPV	1.85	7.25		8.87	10
	CFS	5.54	8.38		9.32	
	OWI	7.37	8.26		9.18	
	HWRF	6.36	8.64		9.4	

Note. Minimum atmospheric pressure error, pressure time series errors, and wind speed time series errors are shown. Units are as denoted except for E_{NORM}. *N* represents sample size. Lowest errors are underlined.

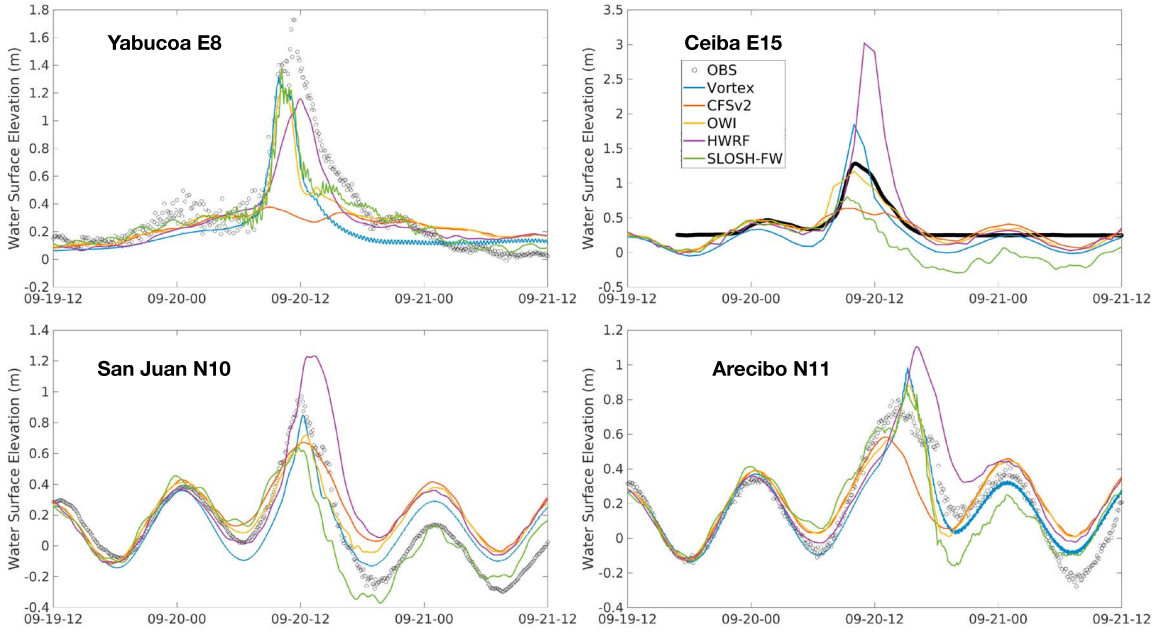

Figure 20. Modeled ADCIRC+SWAN (forced by all wind products) and SLOSH-FW (forced by OWI, and with ADCIRC-computed tides added) water surface elevation time series compared to observed data at a selection of NOAA/NOS water level gauges and a USGS rapid deployment water level gauge during Hurricane Maria.

model fidelity that can be achieved by embedding a higher resolution vortex model into the background atmospheric forcing.

As mentioned in section 3.1, the largest magnitude storm surges from Hurricane Maria appear to be mostly pressure driven, occurring in the southeast and northwest coasts of PR. The most accurate representation of the minimum pressure is captured by OWI and AHPV. The HWRF minimum pressure is too low, while it is too high in the CFSv2 model. The HWRF forced run leads to significant overprediction of the peak surges. A possible source of error in HWRF is that the model has a minimum storm eye wall size of 19 km (Biswas et al., 2017), which is larger than the estimated 16-km eye diameter of Hurricane Maria prior to landfall in PR (Pasch et al., 2018). All of the models estimate that the peak minimum pressure occurs later (0.9–3.5 hr) than observed.

In terms of wave characteristics, the OWI forced simulation had the smallest time series errors for significant wave height and mean wave period. The wave direction error metrics are lowest for HWRF; however, OWI has the second lowest and performs comparably (Figure 21). This shows that overall, for Hurricane Maria across all of the important model response metrics, the OWI forcing performs the best and most consistently. The combination of far-field winds and a detailed representation of the Hurricane itself allow the OWI forced simulation to capture the most complete picture of the wave environment.

3.3. Storm Surge and Wave Model Comparison

3.3.1. Hurricane Irma

Comparing the ADCIRC+SWAN and SLOSH-FW models highlights how model resolution, computational domain size, and intrinsic dissipation impacts the physics of hurricane-induced water levels and wave fields. In addition to Figures 22 and 23, the Hurricane Irma ADCIRC+SWAN to SLOSH-FW comparisons are based on the analysis of Figure 6 compared to Figure S3, and Figures 7 compared to Figure S4; and Figure S5. The coarser SLOSH-FW model has larger maximum water surface elevations in the Virgin Islands and a lower maximum pressure-driven water surface elevation along the track of the storm to the north of PR (Figure 22). The pressure-driven contributions to water levels at the coastal stations are similar between the models (Figures 23) except for certain stations where nonphysical oscillations in the SLOSH-FW model affect the timing and magnitude of peak surge such as Mayaguez on the west coast of PR (Figure 17).

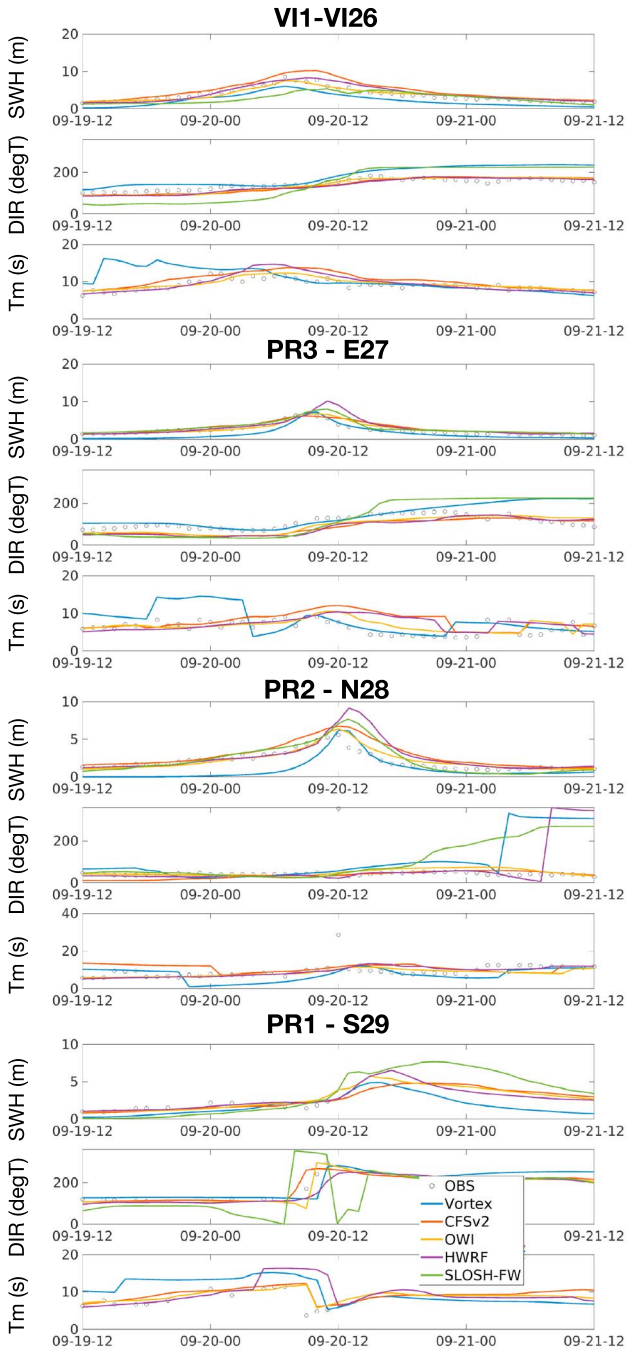

Figure 21. Modeled ADCIRC+SWAN (forced by all wind products) and SLOSH-FW (forced by OWI) significant wave height and direction time series compared to observed data at a CARICOOS wave gauges during Hurricane Maria. Mean wave period comparisons are shown for the ADCIRC+SWAN runs. PR = Puerto Rico.

Generally, there is a domain-wide decrease in maximum water surface elevation due to winds in the SLOSH-FW model that is not present in the ADCIRC+SWAN simulations (Figures 6). This is likely due to the artificial 100-m depth limiting applied across the entire SLOSH-FW computational domain for the purposes of numerical stability The primary specific location where wind-induced surges differ is along the east coast of PR, where winds in the SLOSH-FW model have a greater positive influence on water levels (Figure 23). In fact, winds in ADCIRC+SWAN have a negative influence of water levels at Culebra and Fajardo, and a smaller positive influence at Isabel Segunda (Figure 6). This highlights the effect that the reef

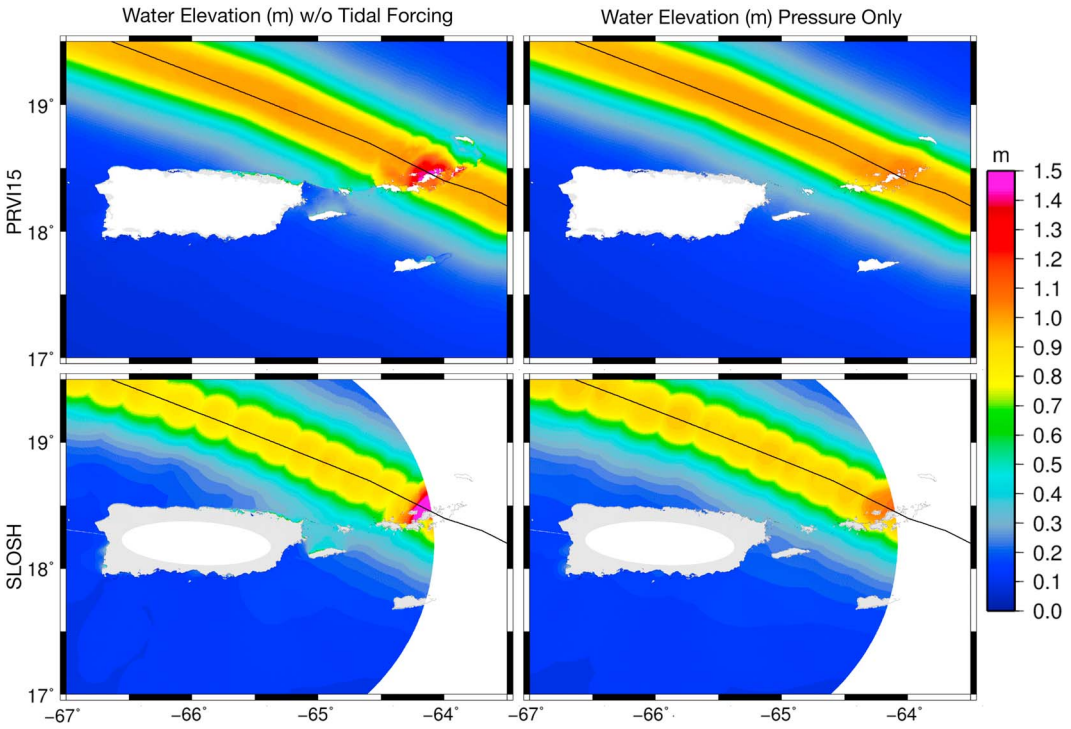

Figure 22. Column 1 shows maximum water surface elevation for Hurricane Irma from a ADCIRC+SWAN coupled run without tides on the high-resolution PRVI15 mesh (top) and from a SLOSH-FW run (bottom). Column 2 shows maximum water surface elevation for Hurricane Irma for a ADCIRC run forced only with atmospheric pressure on the high-resolution PRVI15 mesh (top) and from a SLOSH-FW run (bottom).

system can have on the development of wind-driven surge as it effectively acts to block the development of this surge in the ADCIRC+SWAN model in which the reef system has been highly resolved.

At stations to the east of PR and on Vieques, particularly Fajardo and Isabel Segunda, the wave setup is larger in the SLOSH-FW model (Figure 23) since the reef system to the north of this area that induces wave breaking is not as finely resolved as in the PRVI15 mesh (Figure 3). Therefore, the wave breaking occurs over the shelf instead of at the reef system north of the shelf. On the other hand, the wave-induced contribution to maximum water levels is up to 20 cm less in the SLOSH-FW model along the northern PR coast (Figure S3).

Most differences in tidal contributions between the two models can be attributed to differences in other forcing components (wind, wave, or pressure effects) between the two models that lead to the peak surge occurring at different times in the tidal cycle. This effect is most pronounced at Esperanza, Fajardo, and Culebra (Figure S5).

Overall, the Hurricane Irma peak surge error metrics across all stations for the SLOSH-FW model are slightly better than the ADCIRC+SWAN model (Table 4). SLOSH-FW has smaller values of *MAE* and E_{NORM}, while $\bar{E}$ in ADCIRC+SWAN is superior. However, there are noticeable nonphysical oscillations, visible in Figure 17, which occur in the SLOSH-FW water surface elevation fields, and these affect the determination of peak storm surge at a number of stations. This is particularly clear at Mayaguez and Magueyes, where the pressure contribution in SLOSH-FW is larger than the pressure contribution at San Juan (Figure 23), despite being significantly further away from the eye of the storm leading to larger peak water levels than ADCIRC+SWAN. These oscillations also affect the water surface elevation time series errors at the stations. Despite having lower HWM errors, the overall water surface elevation time series *MAE* and *RMSE* are slightly higher for SLOSH-FW (0.09 and 0.09 m) compared to ADCIRC+SWAN (0.07 and 0.07 m).

Simulation of the large wave heights north of PR appear qualitatively similar between the two models. The error in significant wave height is larger in FW ($MAE = 0.95$ m and $RMSE = 1.18$ m) compared to SWAN ($MAE = 0.32$ m and $RMSE = 0.45$ m). In some cases, the wave heights and directions from FW are clearly less accurate. This particularly occurs at the VI1 station, which is on the eastern edge of the wave model

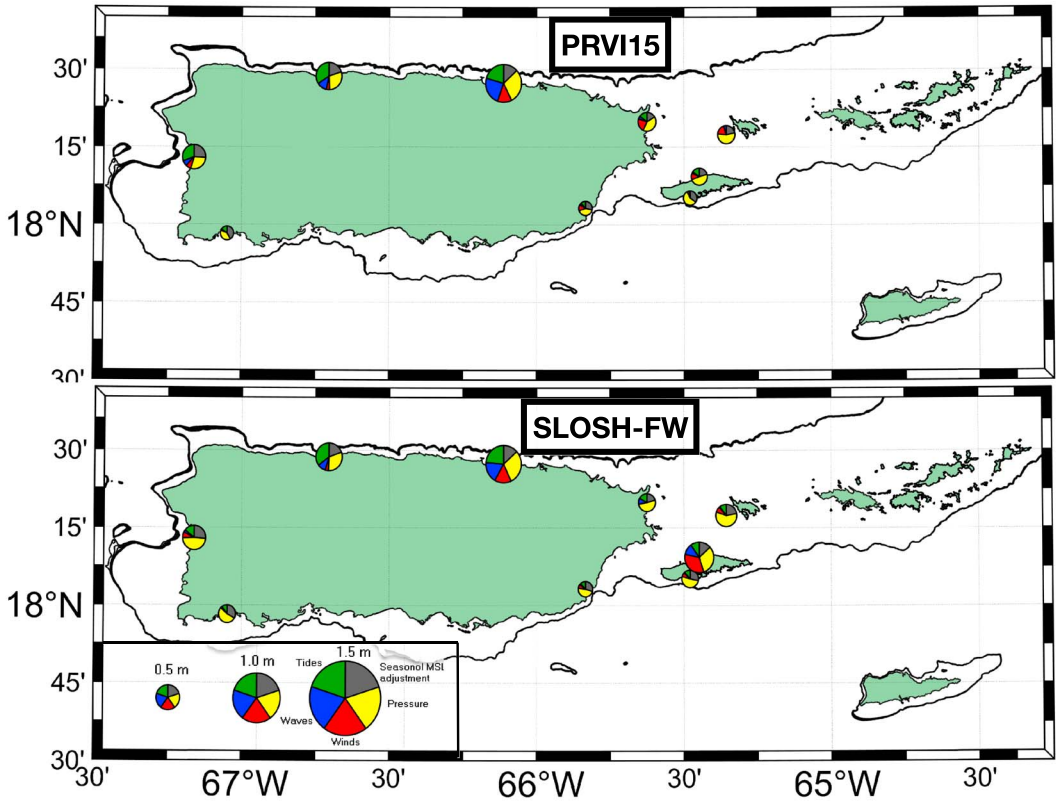

Figure 23. The absolute contribution from the main forcing components (winds, waves, pressure, and tides) in ADCIRC+SWAN (top) and SLOSH-FW (bottom) to the peak surge in the Hurricane Irma simulations. Each pie chart represents a station with the size scaled to the peak surge that occurred at that station. The 100- to 200-m bathymetric contour is highlighted showing the location of the island shelves.

domain. Because of the limited domain, and the omission of offshore wave boundary conditions, hurricane swell waves to the S-SE generated outside of the SLOSH-FW domain are not included. As a result, the early-onset wave heights are underestimated, and wave directions here are inaccurate (Table 4 and Figure 16). The wave-induced forces (not shown) occur in similar areas, at similar times with similar magnitudes between the two models. Despite these similar wave forces between SWAN and FW, the resulting wave setup is smaller in the SLOSH water level fields along the north shore of PR (Figure 23).

3.3.2. Hurricane Maria

In addition to Figures 24 and 25, the Hurricane Maria ADCIRC+SWAN to SLOSH-FW comparisons are based on the analysis of Figure 6 compared to Figure S3, and Figure 10 compared to Figure S6; and Figure S7. Compared to ADCIRC+SWAN the maximum water levels in the SLOSH-FW model are weaker along the track of the storm where the increased water levels are pressure-driven but slightly larger over the eastern PR and USVI shelf (Figure 24). At stations close to the storm track, pressure dominates the peak surge in the southeast and northwest corners of the island in both models (Figure 25). Here, the pressure-driven contribution is weaker in the SLOSH-FW model. On the other hand, the pressure contribution is comparable at the easternmost stations (Lameshur Bay and Culebra) where the peak surge is small.

The spatial distribution of the wind-driven contribution to peak surge at the stations is similar between the two models but is generally larger in the ADCIRC+SWAN simulation (Figure 25). This is particularly evident on the eastern PR shelf where the largest wind-driven setup occurs such as at Fajardo and Ceiba. One reason for this large difference could be the effect that the reef system has in trapping surge over the shelf and along the eastern coast of PR as described in section 3.1. This effect is represented in the ADCIRC+SWAN model, but not in SLOSH-FW due to resolution disparities. In comparison, the north side of the PR exhibits a small amount of wind-driven surge due to the narrow shelf leading to minor differences between the two models. Along the southern coastline of PR the wind-driven surges are on the order of 0.10 to 0.20 m (Figure S3) and the differences between the two models are smaller in magnitude than along the eastern coast (Figure 25).

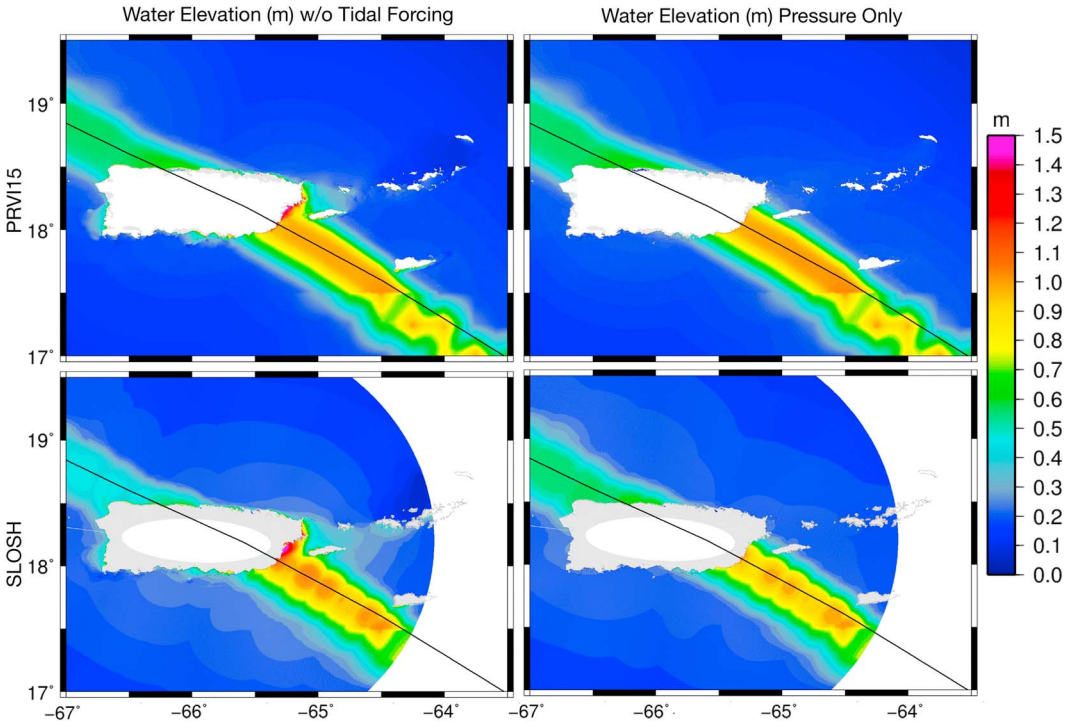

Figure 24. Column one shows maximum water surface elevation for Hurricane Maria from a ADCIRC+SWAN coupled run without tides on the PRVI15 mesh (top) and from a SLOSH-FW run (bottom). Column two shows maximum water surface elevation for Hurricane Maria for a ADCIRC run forced only with atmospheric pressure on the PRVI15 mesh (top) and from a SLOSH-FW run (bottom).

One of the most noticeable differences between the two models is a wind-driven increase to maximum water levels southeast off the PR shelf as the storm approaches, and a decrease in the wake of Hurricane Maria on the north west corner of PR for the SLOSH-FW model (Figure S3) that is not present in ADCIRC+SWAN (Figure 6). Interestingly, tide gauge observations show a poststorm decrease in the base water levels around the island after the passage of Hurricane Maria. However, this decrease persists significantly longer (weeks instead of hours) in the observed data than in the SLOSH-FW model (see specifically San Juan and Arecibo in Figure 20). Additionally, a similar wind-driven trough occurs in the trail of the Hurricane Irma SLOSH-FW simulations while it does not occur in the observed data after that storm. By altering the depths in the PRVI15 mesh in the study region to resemble the maximum 100-m depth found in the SLOSH-FW model, this effect was recreated using the ADCIRC+SWAN model (not shown). Artificial depth limiting performed for numerical stability purposes in SLOSH-FW can lead to unrealistic wind-driven effects off the shelf which in turn affect coastal water levels. Thus, depending on the storm track SLOSH-FW may erroneously compute wind-driven surge in the open ocean adjacent to narrow-shelved island environments. Note that the post storm drawdown in the water level data can be attributed to vertical mixing and cold water upwelling due to the passage of Hurricane Maria over the Puerto Rican shelf, which was reproduced when incorporating baroclinicity into ADCIRC (Pringle et al., 2019). Observations at the CARICOOS San Juan buoy documented these dynamics, with ocean temperature dropping almost 5°, and an increase in salinity from 35.5 to 37.3 psu (Chardon-Maldonado et al., 2018). Since Hurricane Irma passed to the north of the Puerto Rican shelf over deep water, setdown in the water level was not observed in the study region for this storm (Pringle et al., 2019).

The general effect of waves on maximum surge in SLOSH-FW is smaller at the coastline in the study region and much of the set down seen in the ADCIRC+SWAN model over the eastern Puerto Rico shelf (Figure 6) is not present in SLOSH-FW (Figure S3). The greatest difference in wave effect occurs at the USGS stations on the southern PR coast (Santa Isabel, Juana Diaz, and Ponce), where ADCIRC+SWAN has approximately 0.20 m of wave setup and SLOSH-FW has little wave-induced contribution (Figure 25), and total peak surge is considerably smaller at these stations for the SLOSH-FW model. The coarser resolution of SLOSH-FW over the shelf break and reef systems in eastern PR means that waves do not break offshore leading to wave

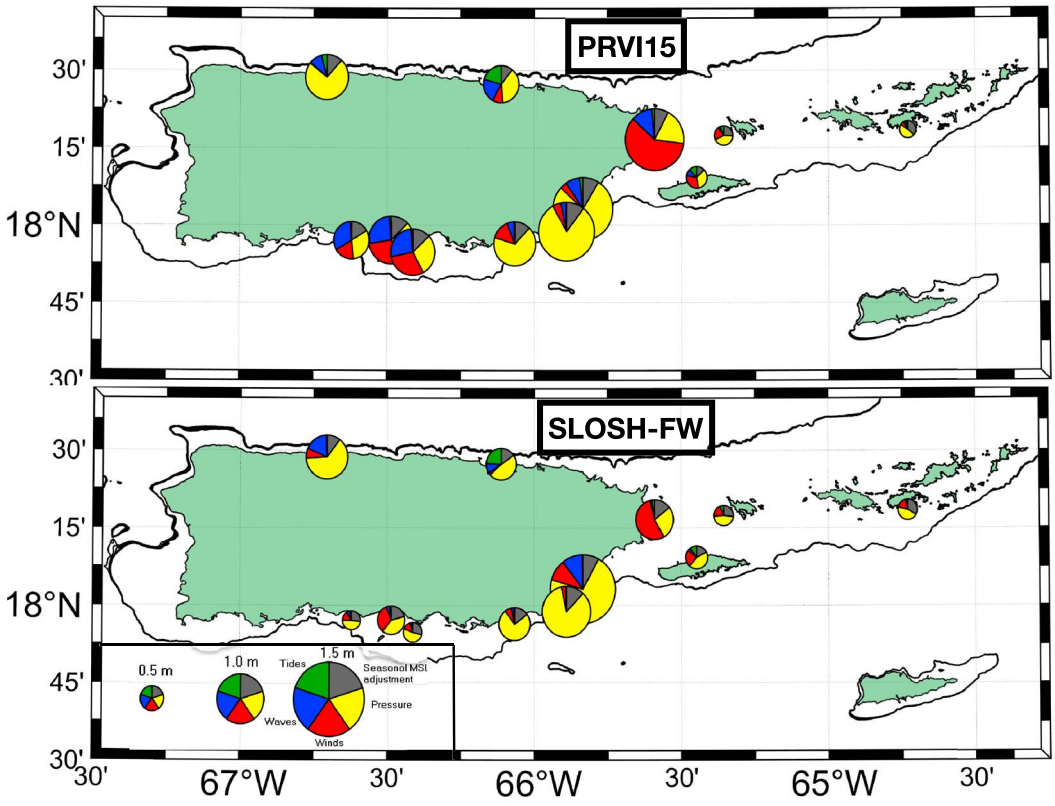

Figure 25. The absolute contribution from the main forcing components (winds, waves, pressure and tides) in ADCIRC+SWAN (top) and SLOSH-FW (bottom) to the peak surge in the Hurricane Maria simulations. Each pie chart represents a station with the size scaled to the peak surge which occurred at that station. The 100- to 200-m bathymetric contour is highlighted showing the location of the island shelves.

growth here as in ADCIRC+SWAN (section 3.1). This effect is clear in the contribution to peak surge at Isabel Segunda and Ceiba (Figures 25), where instead of a wave-induced setdown at these locations, the effect of waves is smaller and/or positive for SLOSH-FW (Figures S3 and S7). Along the north side of the island the wave-driven surge differs slightly, as the wave setup is larger at San Juan in the ADCIRC+SWAN model and larger in the SLOSH-FW model at Arecibo (Figure 25). The wave-induced setup on the southeast facing sides of the islands of St. Croix and Vieques is noticeably smaller in SLOSH-FW. At St. Croix this is likely due to the proximity of the islands to the SLOSH model boundary, while at Vieques, it may be due to a difference in grid resolution between the two models at the island as the SLOSH-FW is unable to sufficiently resolve the wave breaking and resulting setup detailed in section 3.1.

As with Hurricane Irma, most differences in tidal contributions between the two models can be attributed to differences in other forcing components (wind, wave, or pressure effects) between the two models that lead to the peak surge occuring at different times in the tidal cycle. This effect is most pronounced at Fajardo and Ceiba where there is significantly more wind-driven surge in the ADCIRC+SWAN model.

There is a larger difference in the peak surge errors ($\bar{E}$ and *MAE*), shown in Table 6, between the two models for Hurricane Maria compared to Irma, coinciding with the larger coastal surges that occurred during Maria. The mean measured peak surge for Hurricane Maria across all stations was 1.04 m (compared to 0.52 m for Hurricane Irma), the mean peak surge error was −0.36 m for SLOSH-FW and −0.20 m for ADCIRC+SWAN. Much of the difference can be attributed to differences in the wind- and wave-induced setup between the models (Figure 25). The largest differences in modeled peak surges at validation points are found at the USGS rapid deployment gauges which are located further inland than the NOAA gauges. Here, the ADCIRC+SWAN-modeled water levels are significantly larger and more closely match observations. Many of these stations lie along the southern PR coast where wave setup is smaller in the SLOSH-FW model. Overall, the E_{NORM} is smaller in the PRVI15 model (0.28) than for SLOSH-FW (0.38).

Table 6
Hurricane Maria Model Response Errors for All the ADCIRC+SWAN PRVI15 Model With All Atmospheric Forcings and the SLOSH-FW Model Forced With OWI and With ADCIRC Tides Added

Maria response	Simulation	$\bar{E}$	*MAE*	E_{NORM}	*RMSE*	*N*
HWM timing (hours)	AHPV	−0.14	1.36			14
	CFS	1.02	3.97			
	OWI	−0.20	1.67			
	HWRF	0.8	1.75			
	SLOSH-FW	0.7	1.58			
HWM (m)	AHPV	−0.04	0.36	0.35		14
	CFS	−0.48	0.48	0.41		
	OWI	−0.2	0.28	0.26		
	HWRF	0.37	0.51	0.53		
	SLOSH-FW	−0.36	0.38	0.37		
WSE (m)	AHPV	−0.183	0.22		0.253	14
	CFS	−0.11	0.189		0.247	
	OWI	−0.109	0.176		0.214	
	HWRF	−0.025	0.226		0.317	
	SLOSH-FW	−0.205	0.257		0.296	
SWH (m)	AHPV	−0.88	1.01		1.17	4
	CFS	0.09	0.46		0.72	
	OWI	−0.08	0.35		0.54	
	HWRF	0.10	0.48		0.86	
	SLOSH-FW	−0.07	1.08		1.45	
Wave direction (deg)	AHPV		47.45		64.52	4
	CFS		29.13		45.65	
	OWI		25.73		44.18	
	HWRF		20.33		30.30	
	SLOSH-FW		66.03		79.07	
Mean wave period (s)	AHPV	3.15	4.51		5.88	4
	CFS	0.21	2.22		3.03	
	OWI	−0.81	1.75		2.51	
	HWRF	−0.75	1.98		2.67	
	SLOSH-FW					

Note. Peak surge (HWM) error, water surface elevation time series, and wave property (significant wave height, SWH, wave direction, and mean wave period) time series are shown. Units are as denoted except for E_{NORM}. *N* represents sample size. Lowest errors are underlined.

The error discrepancies in the wave response are similar to those found in the Hurricane Irma comparison. Table 6 shows that the error in significant wave height error is larger in the SLOSH-FW model (*MAE* = 1.08 m and *RMSE* = 1.45 m) compared to the ADCIRC+SWAN run (*MAE* = 0.35 m and *RMSE* = 0.54 m). As with Hurricane Irma, the largest errors in the significant wave height and direction are found at station VI1, located on the eastern model boundary, due to the omission of far-field wave components.

4. Discussion

The high-resolution (~30–100 m at the PR and USVI coast) coupled ADCIRC+SWAN+OWI model was run with a number of different forcing configurations to estimate relative response contributions of tides, winds, pressure, and wind wave setup or setdown on simulated water levels. Based on these model analyses the storm surge from both hurricanes was predominantly driven by the inverted barometer response to low atmospheric pressure due to the narrow-shelved environment and strong central minimum pressures. However, wind-driven surge was important in very specific areas of the region. The shelf to the east of PR, connecting PR to USVI is broad enough that during Hurricane Maria a moderate amount of surge

attributable to winds developed to the east of PR and Vieques Island. Additionally, features like the reef system on the north side of the shelf to the east of PR interacted with the wind-driven surge. During Hurricane Irma, this feature halted the passage of water that was being directed from the northern portion of the shelf toward the PR east coast and Vieques. However, during Hurricane Maria, this feature had the opposite effect on wind-driven coastal water levels, trapping wind-driven surge that developed of the eastern PR shelf against the island, not allowing it to escape to the north and piling up water on the northeastern corner of PR. The larger tidal range on the Atlantic side of the islands also played a role in the high water levels along the north side of the island for both storms. During the period of time when the storms were having their largest impact on coastal water levels, large portions of the north side of PR in particular were experiencing high tides.

Both storms induced waves in excess of 10 m in the PR and USVI region, contributing to wave setup which was most prominent on the north side of PR during Hurricane Irma and both the north and south sides of PR during Hurricane Maria. There are very narrow shelves and steep bathymetric gradients on these sides of the island and the over 10-m waves breaking in such close proximity to the coast had a large effect on coastal water levels. In spots this exceeded 40 cm and a quarter of the total water level increase. Setdown east of PR and north of USVI due to wave growth was also apparent during Hurricanes Maria and Irma, respectively. This wave growth occurred due to the large waves being dissipated at the shelf break and along reef structures. The wave heights were therefore small enough over the shelf to not immediately break, but instead grow. The appearance of these wave growth-associated setdowns highlight the importance of including model resolution that sufficiently captures shelf breaks, reef structures, and other nearshore features that cause the dissipation of wave energy. This is particularly true in regions like the Caribbean where there is no broad continental shelf to attenuate wave heights before they approach the nearshore.

The comparison of atmospheric forcing models on coastal water levels and wind wave conditions highlighted the following. The AHPV model based on ATCF best-track data accurately represents storm characteristics within the radius of both hurricanes Irma and Maria while missing far-field information. The OWI fields, which embed a PBL vortex model into a synoptic scale model, provides more accurate surge and wave results in areas farther away from the radius of maximum winds. This becomes important in an archipelago such as PR and USVI where severe coastal damage can occur in distant areas from the radius of maximum winds as was the case in the San Juan Bay area (northeast PR) during Hurricane Irma. Interestingly, even though HWRF embeds a storm-centered dynamic core into two larger scale domains, it did not result in a more accurate representation of the hurricane field. Recent studies have indicated that assimilation of ocean glider data (Dong et al., 2017) and incorporation of RTOFS temperature and salinity fields (Kim et al., 2018) has resulted in better HWRF performance. These strategies should be explored in future HWRF development in the PR and USVI region.

Comparisons of ADCIRC+SWAN, simulated on a regional-scale western North Atlantic Ocean mesh, and SLOSH-FW, simulated on a local-scale mesh, highlighted the following. During Hurricane Irma where surge was relatively small at the PR and USVI gauges ($N = 10$), the mean error in the peak surge (HWM) was smallest in the SLOSH-FW model, but the ADCIRC+SWAN model performed better on a total time series basis. It is noted that nonphysical oscillations in the SLOSH-FW response affected errors for that model both positively and negatively. In general, the storm surge was modest for Hurricane Irma, almost always less than 1 m with an average of 0.52 m at observation stations. During Hurricane Maria where surge at the PR and USVI gauges ($N = 14$) was more significant, the mean HWM error was smaller for ADCIRC+SWAN ($E_{\mathrm{NORM}} = 0.26$) than SLOSH-FW ($E_{\mathrm{NORM}} = 0.37$). It was only in the wide shelved region to the east of PR during Hurricane Maria that storm surge reached at least 1.6 m. Both ADCIRC+SWAN and SLOSH-FW generally represent peak surge due to the dominant atmospheric pressure and smaller wind-driven component similarly accurately over the PR and USVI shelf. This is in comparison to simulations over broad shelves, where wind-driven surge is dominant and in return the bottom friction treatment in SLOSH tends to underestimate hurricane forerunner contributions (Kerr, Donahue, et al.,2013). Poststorm erroneous wind-driven setdown was observed in the SLOSH simulations due to ocean depths being limited to 100 m, which causes problems in predicting surge depending on the storm track.

Wind-driven waves are significant in steep-shelved island environments leading to wave-induced setup (considered here) and run-up (not considered here). ADCIRC+SWAN simulates greater wave setup compared to SLOSH-FW along many of the PR and USVI coastlines (including the south side of PR dur-

ing Hurricane Maria) where wave breaking occurs over steep bathymetry and reef systems. This is mainly a function of resolution in the SLOSH-FW model which insufficiently resolves the nearshore features that are important for wave breaking causing setup. For similar reasons, reef edge wave breaking over the east of PR and subsequent wave growth did not occur in SLOSH-FW during Hurricane Maria. As a result, the setdown that was observed in ADCIRC-SWAN was not seen in the SLOSH-FW model. On the south coast of PR significant differences in wave setup led to large differences with regard to on-land inundation. Apart from model resolution, the limited extent of the SLOSH-FW domain also affects its performance in some areas. This is especially the case at the USVI on the eastern boundary, where the contributions of far-field hurricane-induced swells are not accounted for, leading to an underprediction of early wave heights and inaccurate wave directions.

Finally, there are three major physical processes ignored in the study that may be considered important for steep-sloped island environments and should be included in future modeling of the region. The first is wave run-up and overtopping causing coastal flooding, identified as a significant factor in Hawaii (Kennedy et al., 2012). Second, heavy rainfall causing flooding was critical in Hurricane Maria (Pasch et al., 2018), thus coupling coastal models to hydrological models (e.g., Silva-Araya et al., 2018) and identifying areas susceptible to rain-induced flooding, coastal flooding, or a combination of both (Bilskie & Hagen, 2018), is an important step going forward. Last, the density structure of the ocean accounts for a reasonably large proportion of sea level variability in the Caribbean, and incorporating baroclinicity through coupling to data-assimilated global ocean models (e.g., GOFS 3.1; Metzger et al., 2017) has been shown to improve depth-integrated model skill in comparison to coastal sea level observations around PR and USVI (Pringle et al., 2019).

5. Conclusions

The IOOS-funded COMT project has the goal of improving operational storm surge and wind wave modeling capabilities in deep ocean island environments. As part of the COMT project, high-resolution surge, tide, and wind wave hindcast simulations of Hurricanes Irma (2017) and Maria (2017) were conducted due to their significant and devastating recent impact on the PR and USVI region, and the amount of data available to support the validation of meteorological forcing, water levels and waves. A preferred configuration of coastal circulation (ADCIRC), wind wave (SWAN), and atmospheric (OWI) models was employed to conduct most of the analysis. Comparisons between meteorological forcing models (OWI, AHPV, CFSv2, and HWRF) and the simplified experimental surge and wind wave model, SLOSH-FW, were undertaken to assess the importance of model aspects for the region.

The main conclusions from this study are as follows:

1. Since wind-drive surge is not dominant in the steep-sloped island environment, it is paramount that the components of the total coastal water level (inverted barometer response to atmospheric pressure, tides, wind-driven surge, wind-/wave-induced setup, and baroclinically driven mean sea level offset) are all equally considered to obtain high-fidelity forecast accuracy. The importance of high spatial resolution and detail of dissipative structures such as reefs, shoals, and banks to adequately model components such as wind-driven surge and wave setup was demonstrated through ADCIRC+SWAN simulations on the PRVI15 model.
2. Parametric vortex models are adequate to assess hurricane-induced water levels at coastal locations in the direct path of hurricane where pressure-driven effects dominate, but not elsewhere, and wind wave conditions and hence wave setup will be deficient in general. Embedding vortex models into synoptic scale winds (e.g., OWI) and/or improving assimilation of ocean temperature and salinity fields for HWRF is recommended.
3. Small-scale models (SLOSH) that are sufficiently resolved (~200 m at the coast) appear largely adequate to represent the response to atmospheric pressure and winds in PR and USVI. However, numerical oscillations develop that likely originate from the open boundaries which cannot be dissipated away due to the narrow shelf. This is despite the fact that ocean depths were limited 100 m in SLOSH which leads to the generation of unphysical wind-driven surge and an artificial trough in water levels in the trail of the storm.
4. For Hurricane Maria, in particular, the importance of wave-current interaction was highlighted. Compared to SWAN and wave buoy observations, the simplified wave model FW performed well in computing

wave properties. However, the coupled SLOSH-FW model significantly underestimated wave setup effects at the coastline compared to ADCIRC+SWAN due to the low grid resolution (1 km) of FW.

5. The importance of high spatial resolution and detail of dissipative structures such as reefs, shoals, and banks is shown through the comparison of the PRVI15 and HSOFS unstructured meshes. Under the same OWI atmospheric forcing, the higher resolution PRVI15 mesh provides a notable improvement in performance for both hurricanes. The most noticeable effect was the generation of surge due to wave setup, which PRVI15 captured for both hurricanes, while HSOFS both underestimated and overestimated surge due to its lower spatial resolution. Geometric representation of the shelf width is also important, in which disparities resulted in water level differences of more than 50% in some locations.

Acknowledgments

This work was sponsored through a grant managed by the Southeastern Universities Research Association (SURA), award NA13NOS0120139, and funded by the U.S. IOOS Coastal and Ocean Modeling Testbed. J. J. Westerink was also supported in part by the Joseph and Nona Ahearn endowment at the University of Notre Dame. The authors also acknowledge the CARICOOS (https://www.caricoos.org/) and USGS teams for developing the operational and deployed systems that collected critical observations during Hurricanes Irma and Maria. All data used for the production of the results contained in this paper will be hosted on the Integrated Ocean Observing System Coastal Ocean Modeling Testbed webpage under the Puerto Rico/U.S. Virgin Islands Storm Surge and Waves project. All data used for validation can be accessed as listed in the manuscript.

References

Becker, J. J., Sandwell, D. T., Smith, W. H. F., Braud, J., Binder, B., Depner, J., et al. (2009). Global bathymetry and elevation data at 30 arc seconds resolution: SRTM30_PLUS. *Marine Geodesy*, *32*(4), 355–371. https://doi.org/10.1080/01490410903297766

Bilskie, M. V., & Hagen, S. C. (2018). Defining flood zone transitions in low-gradient coastal regions. *Geophysical Research Letters*, *45*, 2761–2770. https://doi.org/10.1002/2018GL077524

Bilskie, M. V., Hagen, S. C., Medeiros, S. C., Cox, A. T., Salisbury, M., & Coggin, D. (2016). Data and numerical analysis of astronomic tides, wind-waves, and hurricane storm surge along the northern Gulf of Mexico. *Journal of Geophysical Research: Oceans*, *121*, 3625–3658. https://doi.org/10.1002/2015JC011400

Biswas, M. K., Bernardet, L., Abarca, S., Ginis, I., Grell, E., Kalina, E., et al. (2017). Hurricane Weather Research and Forecasting (HWRF) model: 2017 scientific documentation (NCAR Technical Note NCAR/TN-544+STR). National Center for Atmospheric Research. https://doi.org/10.5065/D6MK6BPR

Booij, N., Ris, R. C., & Holthuijsen, L. H. (1999). A third-generation wave model for coastal regions: 1. Model description and validation. *Journal of Geophysical Research*, *104*(C4), 7649–7666. https://doi.org/10.1029/98JC02622

Canals, M., & Morell, J. (2015). A nearshore breaker prediction system for Puerto Rico and the United States Virgin Islands in support of beach safety and drowning prevention, *OCEANS'15 MTS/IEEE Washington* (pp. 1–10). Washington, DC: IEEE.

Canals, M., Morell, J., Corredor, J. E., & Leonardi, S. (2012). Expanding the Caribbean coastal ocean observing system into the nearshore region, *Oceans, 2012* (pp. 1–4). Virginia Beach, VA: IEEE.

Cangialosi, J. P., Latto, A. S., & Berg, R. (2018). National hurricane center tropical cyclone report—Hurricane Irma. AL112017.

Chardon-Maldonado, P., Fleming, R., & Wallinga, J. (2018). Riders on the Storm—CARICOOS moored oceanographic data buoys during the 2017 hurricane season. In *OCEANS 2018-Kobe*. IEEE.

Chen, C., Beardsley, R. C., Luettich, R. A. Jr., Westerink, J. J., Wang, H., Perrie, W., et al. (2013). Extratropical storm inundation testbed: Intermodel comparisons in Scituate, Massachusetts. *Journal of Geophysical Research: Oceans*, *118*, 5054–5073. https://doi.org/10.1002/jgrc.20397

Cox, A., Callahan, B., Ferguson, M., & Morrone, A. (2017). *Tropical cyclone wind*. Liverpool, UK: 1st International Workshop on Waves, Storm Surges and Coastal Hazards.

Dietrich, J. C., Tanaka, S., Westerink, J. J., Dawson, C. N., Luettich, R. A., Zijlema, M., et al. (2012). Performance of the unstructured-Mesh, SWAN+ADCIRC Model in computing hurricane waves and surge. *Journal of Scientific Computing*, *52*(2), 468–497. https://doi.org/ 10.1007/s10915-011-9555-6

Dietrich, J. C., Zijlema, M., Allier, P.-E., Holthuijsen, L. H., Booij, N., Meixner, J. D., et al. (2013). Limiters for spectral propagation velocities in SWAN. *Ocean Modelling*, *70*, 85–102.

Dietrich, J., Zijlema, M., Westerink, J., Holthuijsen, L., Dawson, C., Luettich, R., et al. (2011). Modeling hurricane waves and storm surge using integrally-coupled, scalable computations. *Coastal Engineering*, *58*(1), 45–65. https://doi.org/10.1016/j.coastaleng.2010.08.001

Dong, J., Domingues, R., Goni, G., Halliwell, G., Kim, H.-S., Lee, S.-K., et al. (2017). Impact of assimilating underwater glider data on Hurricane Gonzalo (2014) forecasts. *Weather and Forecasting*, *32*(3), 1143–1159.

Egbert, G. D., Bennett, A. F., & Foreman, M. G. G. (1994). TOPEX/POSEIDON tides estimated using a global inverse model. *Journal of Geophysical Research*, *99*(C12), 24,821–24,852. https://doi.org/10.1029/94JC01894

Ferreira, C. M., Irish, J. L., & Olivera, F. (2014). Uncertainty in hurricane surge simulation due to land cover specification. *Journal of Geophysical Research: Oceans*, *119*, 1812–1827. https://doi.org/10.1002/2013JC009604

Garratt, J. R. (1977). Review of drag coefficients over oceans and continents. *Monthly Weather Review*, *105*(7), 915–929. https://doi.org/10.1175/1520-0493(1977)105<0915:RODCOO>2.0.CO;2

Giri, C., Ochieng, E., Tieszen, L. L., Zhu, Z., Singh, A., Loveland, T., et al. (2011). Status and distribution of mangrove forests of the world using earth observation satellite data. *Global Ecology and Biogeography*, *20*(1), 154–159. https://doi.org/10.1111/j.1466-8238.2010.00584.x

Gonzalez-Lopez, J., Pomales, L., Garcia-Moreno, C., Seijo, G., Solano, M., Morell, J., et al. (2017). Incorporating HF-radar and Lagrangian drifters into a coastal and mesoscale model validation framework in the eastern Caribbean Sea. In *99th AMS Annual Meeting*. Seattle, Washington.

Hope, M. E., Westerink, J. J., Kennedy, A. B., Kerr, P. C., Dietrich, J. C., Dawson, C., et al. (2013). Hindcast and validation of Hurricane Ike (2008) waves, forerunner, and storm surge. *Journal of Geophysical Research: Oceans*, *118*, 4424–4460. https://doi.org/10.1002/jgrc.20314

Jelesnianski, C. P. (1967). Numerical computations of storm surges with bottom stress. *Monthly Weather Review*, *95*(11), 740–756. https://doi.org/10.1175/1520-0493(1967)095<0740:NCOSSW>2.3.CO;2

Jelesnianski, C. P., Chen, J., & Shaffer, W. A. (1992). SLOSH: Sea, lake, and overland surges from hurricanes (Tech. Rep.). United States, National Weather Service.

Kendall, M., Monaco, M., Buja, K., Christensen, J., Kruer, C., Finkbeiner, M., & Warner, R. (2001). Methods used to map the benthic habitats of Puerto Rico and the U.S. Virgin Islands, *Benthic habitats of Puerto Rico and the U.S. Virgin Islands*. Silver Spring, MD: U.S. National Oceanic and Atmospheric Administration (NOAA). National Ocean Service (NOS), National Centers for Coastal Ocean Science (NOS) Biogeography Program.

Kennedy, A. B., Gravois, U., Zachry, B. C., Westerink, J. J., Hope, M. E., Dietrich, J. C., et al. (2011). Origin of the Hurricane Ike forerunner surge. *Geophysical Research Letters*, *38*, L08608. https://doi.org/10.1029/2011GL047090

Kennedy, A. B., Westerink, J. J., Smith, J. M., Hope, M. E., Hartman, M., Taflanidis, A. A., et al. (2012). Tropical cyclone inundation potential on the Hawaiian islands of Oahu and Kauai. *Ocean Modelling*, *52–53*, 54–68. https://doi.org/10.1016/j.ocemod.2012.04.009

Kerr, P. C., Donahue, A. S., Westerink, J. J., Luettich, R. A., Zheng, L. Y., Weisberg, R. H., et al. (2013). U.S. IOOS coastal and ocean modeling testbed: Inter-model evaluation of tides, waves, and hurricane surge in the Gulf of Mexico. *Journal of Geophysical Research: Oceans*, *118*, 5129–5172. https://doi.org/10.1002/jgrc.20376

Kerr, P. C., Martyr, R. C., Donahue, A. S., Hope, M. E., Westerink, J. J., Luettich, R. A., et al. (2013). U.S. IOOS coastal and ocean modeling testbed: Evaluation of tide, wave, and hurricane surge response sensitivities to mesh resolution and friction in the Gulf of Mexico. *Journal of Geophysical Research: Oceans*, *118*, 4633–4661. https://doi.org/10.1002/jgrc.20305

Kim, H.-S., Halliwell, G. R. Jr., Black, P. G., Bond, S. C. N., Cione, J. J., Dong, J., et al. (2018). Ocean model impact study for improvement of tropical cyclone (TC) Forecasting. In *33rd Conference on Hurricanes and Tropical Meteorology*. Ponte Verda, FL.

Luettich, R. A., & Westerink, J. J. (2004). Formulation and numerical implementation of the 2D/3D ADCIRC finite element model version 44.XX (Tech. Rep.).

Luettich, R. A., Wright, L. D., Nichols, C. R., Baltes, R., Friedrichs, M. A., Kurapov, A., et al. (2017). A test bed for coastal and ocean modeling. *Eos*, *98*.

Luettich, R. A., Wright, L. D., Signell, R., Friedrichs, C., Friedrichs, M., Harding, J., et al. (2013). Introduction to special section on the US IOOS coastal and ocean modeling testbed. *Journal of Geophysical Research: Oceans*, *118*, 6319–6328. https://doi.org/10.1002/2013JC008939

Madsen, O. S., Poon, Y.-K., & Graber, H. C. (1989). Spectral wave attenuation by bottom friction: Theory, *Coastal Engineering 1988* (pp. 492–504). Torremolinos, Spain: American Society of Civil Engineers (ASCE).

Mattocks, C., & Forbes, C. (2008). A real-time, event-triggered storm surge forecasting system for the state of North Carolina. *Ocean Modelling*, *25*(3), 95–119. https://doi.org/10.1016/j.ocemod.2008.06.008

Metzger, E. J., Helber, R., Hogan, P. J., Posey, P. G., Thoppil, P. G., Townsend, L., et al. (2017). Global ocean forecast system 3.1 validation testing (Tech. Rep.). Naval Research Laboratory, Stennis Space Center, MS 39529-5004.

Morell, J. M., Canals, M. F., Capella, J. E., Aponte, L. D., Corredor, J. E., Watlington, R., & Garcia, C. (2015). IOOS-CARICOOS: Past, present and future of a tropical coastal ocean observing system, *OCEANS 2015-Genova* (pp. 1–4). Genova, Italy: IEEE.

Mukai, A., Westerink, J., Luettich, R., & Mark, D. (2002). A tidal constituent database for the western North Atlantic Ocean, Gulf of Mexico and Caribbean Sea (Report ERDC/CHL TR-02-24). Vicksburg, MS: U.S. Army Engineer Research and Development Center.

Pasch, R. J., Penny, A. B., & Berg, R. (2018). National hurricane center tropical cyclone report—Hurricane Maria. al152017.

Pomales-Velázquez, L., Morell, J., Rodriguez-Abudo, S., Canals, M., Capella, J., & Garcia, C. (2015). Characterization of mesoscale eddies and detection of submesoscale eddies derived from satellite imagery and HF radar off the coast of southwestern Perto Rico, *OCEANS'15 MTS/IEEE Washington* (pp. 1–6). Washington, DC: IEEE.

Powell, M. D., Vickery, P. J., & Reinhold, T. A. (2003). Reduced drag coefficient for high wind speeds in tropical cyclones. *Nature*, *422*, 279–283.

Pringle, W., Gonzalez, J., Joyce, B., Westerink, J., & van der Westhuysen, A. J. (2019). Baroclinic coupling improves depth-integrated modeling of coastal sea level variations around Puerto Rico and the U.S. Virgin Islands. *Journal of Geophysical Research: Oceans*. https://doi.org/10.1029/2018JC014682

Rodríguez-Abudo, S., Canals, M., Morell, J., Matos, P., García, C., Pomales, L., & Capellax, J. (2015). Assessing HF radar capabilities to resolve mesoscale eddy interactions with littoral waters, *OCEANS'15 MTS/IEEE Washington* (pp. 1–5). Washington, DC: IEEE.

Ruessink, B., Walstra, D., & Southgate, H. (2003). Calibration and verification of a parametric wave model on barred beaches. *Coastal Engineering*, *48*(3), 139–149. https://doi.org/10.1016/S0378-3839(03)00023-1

Saha, S., Moorthi, S., Wu, X., Wang, J., Nadiga, S., Tripp, P., et al. (2014). The NCEP climate forecast system version 2. *Journal of Climate*, *27*(6), 2185–2208. https://doi.org/10.1175/JCLI-D-12-00823.1

Schwab, D. J., Bennett, J. R., Liu, P. C., & Donelan, M. A. (1984). Application of a simple numerical wave prediction model to Lake Erie. *Journal of Geophysical Research*, *89*(C3), 3586–3592. https://doi.org/10.1029/JC089iC03p03586

Silva-Araya, W. F., Santiago-Collazo, F. L., Gonzalez-Lopez, J., & Maldonado-Maldonado, J. (2018). Dynamic modeling of surface runoff and storm surge during hurricane and tropical storm events. *Hydrology*, *5*(1), 13.

Tanaka, S., Bunya, S., Westerink, J. J., Dawson, C., & Luettich, R. A. (2011). Scalability of an unstructured grid continuous Galerkin based hurricane storm surge model. *Journal of Scientific Computing*, *46*(3), 329–358. https://doi.org/10.1007/s10915-010-9402-1

Taylor, L., Eakins, B., Carignan, K., Warnken, R., Sazonova, T., & Schoolcraft (2008). Digital elevation models of Puerto Rico: Procedures, data sources and analysis (NOAA Technical Memorandum NESDIS NGDC-13). Boulder, CO.

van der Westhuysen, A., Anselmi, C., Calzada, R., Feyen, J., Gonzalez, J., Mercado, A., et al. (2015). A wave, surge, and inundation modeling testbed for Puerto Rico and the US Virgin Islands: Year 1 progress, 95th AMS Annual Meeting (pp. 4–8). Phoenix, AZ.

Wessel, P., & Smith, W. H. F. (1996). A global, self-consistent, hierarchical, high-resolution shoreline database. *Journal of Geophysical Research*, *101*(B4), 8741–8743. https://doi.org/10.1029/96JB00104

Westerink, J. J., Luettich, R. A., Feyen, J. C., Atkinson, J. H., Dawson, C., Roberts, H. J., et al. (2008). A basin- to channel-scale unstructured grid hurricane storm surge model applied to southern Louisiana. *Monthly Weather Review*, *136*(3), 833–864. https://doi.org/10.1175/2007MWR1946.1

Wolanski, E., Mazda, Y., & Ridd, P. (2013). Mangrove Hydrodynamics. In *Tropical Mangrove Ecosystems* (Chap. 3, pp. 43–62): American Geophysical Union (AGU). https://doi.org/10.1029/CE041p0043

Xie, D.-M., Zou, Q.-P., & Cannon, J. W. (2016). Application of SWAN+ADCIRC to tide-surge and wave simulation in Gulf of Maine during Patriot's Day storm. *Water Science and Engineering*, *9*(1), 33–41. https://doi.org/10.1016/j.wse.2016.02.003

Yablonsky, R. M., Ginis, I., Thomas, B., Tallapragada, V., Sheinin, D., & Bernardet, L. (2015). Description and analysis of the ocean component of NOAA's operational Hurricane Weather Research and Forecasting Model (HWRF). *Journal of Atmospheric and Oceanic Technology*, *32*(1), 144–163.

Zheng, L., Weisberg, R. H., Huang, Y., Luettich, R. A., Westerink, J. J., Kerr, P. C., et al. (2013). Implications from the comparisons between two- and three- dimensional model simulations of the Hurricane Ike storm surge. *Journal of Geophysical Research: Oceans*, *118*, 3350–3369. https://doi.org/10.1002/jgrc.20248

Zijlema, M. (2010). Computation of wind-wave spectra in coastal waters with SWAN on unstructured grids. *Coastal Engineering*, *57*(3), 267–277. https://doi.org/10.1016/j.coastaleng.2009.10.011